ADDIS ABABA UNIVERSITY

SCHOOL OF MECHANICAL & INDUSTRIAL ENGINEERING

Wear Analysis of Aluminum Matrix-Titanium dioxide Nano Composite Automotive Cam using FEM

A Thesis submitted to the school of Mechanical & Industrial Engineering of Addis Ababa University in partial fulfillment of the Degree of Masters of Science

In

Mechanical Engineering (Mechanical Design Stream)

By: Rediet Assegid (ID: GSR/2948/07)

Advisor: Dr. Daniel Tilahun

September, 2016

ADDIS ABABA UNIVERSITY

ADDIS ABABA INSTITUTE OF TECHNOLOGY

SCHOOL OF MECHANICAL AND INDUSTRIAL ENGINEERING

Wear Analysis of Aluminum Matrix-Titanium dioxide Nano Composite Automotive Cam using FEM

By: Rediet Assegid

Approved by board of examiners

Mr. Getasew Taddese	_____	_____
Acting Chairman of the school	Signature	Date
Dr. Daniel Tilahun	_____	_____
Advisor	Signature	Date
Mr. Araya Abera	_____	_____
Internal Examiner	Signature	Date
Mr. Mulugeta H/Mariam	_____	_____
External Examiner	Signature	Date

Abstract

The purpose of this project is to identify and compare wear and the weight loss of a light duty engine cam using Nano titanium dioxide reinforced aluminum composite cam with a cam of 4% Nano Silicon Carbide reinforced aluminum composite cam. The weight percent of the Nano TiO_2 is taken to be 4%.

Homogenized property of the Nano TiO_2 aluminum composite cam modeling is shown in detail and done through MatLab. After identifying the property of the composite as a single material, the wear analysis with its round faced follower is done through ABAQUS software 6.14CAE for a given conditions of 200 rpm for 6 hours at a room temperature for half kilograms of load.

The wear results of ABAQUS 6.14CAE on three critical portions of the cam, such as the cam basic circle, cam lobe and cam flank is identified at given conditions.

The weight lost found by ABAQUS at the cam is calculated by Archard's wear law. Result showed at 4%wt of Nano TiO_2- Al cam, it is showen better wear result compared to Nano SiC-Al cam.

Key words – Powder metallurgy, Aluminum matrix Nano composite, TiO_2 nanoparticles, wear, cam.

Acknowledgments

First and for most, I would like to thank the almighty God for my whole family whom I have never lost their support. I would also like to thank my close classmate friends who gave me their genuine support thru class hours.

Afterwards, I want to pass my appreciation and big thanks my advisor who guided me with constructive comments during progress reports and meetings since the beginning of this research.

List of Figures

List of Tables

Nomenclature

K	Bulk Modulus
PM	Powder metallurgy
MMC	Metal Matrix Composites
MMNC	Metal Matrix Nano Composites
E	Elastic Modulus
v	Poisons ratio
G	Shear Modulus
a	Thickness of interphase zone
R_g	Radius of gyration
C_i	Volume fractions of phases
λ_o,η_o	Elastic Lame constants
α, β, γ, k	Cosserat material constants
A_o, b_{oi}	Classical components of the Eshelby tensor
μ	Coefficient of friction
g	Gravitational acceleration
ω	Angular velocity of cam
v	Velocity of follower
θ	Cam angle
b	Half contact width
F	force
L	Contact length

R	Radius of curvature
V	Wear by volume
H	Hardness
W_s	Wear volume per load
t	time
Q	Rate of wear
P	Contact pressure
s	Slippage
h	Wear depth
A	Contacting area

Chapter one

Introduction

1.1 Background

Cam shaft and cams are used to time the addition of intake and exhaust valves, the cam shaft is driven by the crank shaft. The crank shaft has 2:1 crank shaft to cam shaft gear ratio. Cam is used as an indexing device in ON/OFF Load Tap changer device of high voltage transformer and serves as the connector between the indexing head and the power changing gears. A camshaft is usually made of cast iron or forged steel. One cam per valve is used to open and close the valves. The cam surfaces are hardened to obtain adequate life. [1]

Depending on valve and camshaft location, additional members are required to transmit the tappet motion to the valve stem; e.g. in-head valve engines with the camshaft at the side, a push rod and rocker arm are used. [2]

The cam is used to control air and fuel flow into and out of the cylinders, facilitating combustion. A cam forms a significant part of three-element mechanisms. Its profile, dimensions of driving and driven elements define a lifting relation taking into consideration individual deformation ratios and a rigidity of an element for requested operation. During its movement the cam is exposed to effects of significant forces at a contact performing a direct influence on its surface that may result in damaging of contact areas. Such damage becomes evident in form of pitting that develops from small cracks on a surface of a working surface. Therefore a correct choice of material of particular elements in a design of a cam mechanism, especially a cam, is the first presumption for a reliable operation of the mechanism.

In Nature, titanium dioxide exists in three primary phases – anatase, rutile, and brookite – with different sizes of crystal cells in each case. The popularity of titanium dioxide in materials sciences began with the first photo catalytic splitting of water in 1972. [3]

However, in recent years TiO_2 has been used widely for the preparation of different types of nano materials, including nanoparticles, Nano rods, Nano wires, Nano tubes, and mesoporous and Nano porous TiO_2 – containing materials. [4]

- Types of Cam Failure

Cam of different car engines faces different types of failure problems. These are described here bellow;

Dry Wear of Camshaft

Wear is determined as weight losses of the samples as a function of wear test duration and loads. The variation of camshaft profile can capture by a level sensor during the wear. The profile variation must be continuously monitored on the computer screen throughout the tests. It is found that wear mechanisms of the cam surface change along the contact surface and maximum wear value is obtained just at cam tip. [5]

Contact Fatigue

Generally, one surface moves over the other in a rolling motion as in a ball rolling over a race in a ball bearing. The contact geometry and the motion of the rolling elements produce an alternating subsurface shear stress. Subsurface plastic strain builds up with increasing cycles until a crack is generated. [5]

- Engine Cam materials and its' properties

A cam has homogenous mechanical features in its whole volume. Choice of a suitable material depends on a maximum value of a contact pressure in a working cycle of a cam mechanism that has been obtained by calculation from a dynamic solution of a particular cam. [2]

At present, camshafts with chilled cams are made using the upper surface re-melting method. Much research work is also being done on the application of technological ceramics, hard sintered metals and composites. [2]

- Nano Composite materials in this research

The general idea behind the addition of the Nano scale second phase is to create a synergy between the various constituents, such that novel properties capable of meeting or exceeding design expectations can be achieved; The properties of Nano composites rely on a range of variables, particularly the matrix material, which can exhibit Nano scale dimensions, loading, degree of dispersion, size, shape, and orientation of the Nano scale second phase and interactions between the matrix and the second phase. [6]

1.2 Statement of the problem

Existing cam is heavier in weight. Recently the increase in number of environmental problems and petroleum depletion rate has appeared to accelerate becoming severer each year. Therefore the reduction in automotive power - train friction has become necessary in recent years for improving fuel economy. Cam follower friction is 20 – 30% of engine friction.

Good workability and wear problems are shown on the engine cam. During its movement the cam is exposed to effects of significant forces at a contact performing a direct influence on its surface that may result in damaging of contact areas. Such damage becomes evident in form of pitting that develops from small cracks on a surface of a working surface.

Therefore in this research finite element analysis is used to find out single property of the cam and ABAQUS software is used for wear analysis of cam and follower. At the end nano SiC-Al cam will be compared with Nano TiO_2 – Al cam.

1.3 Objective

❖ General objective

- The main objective of this research is to do wear analysis of composite automotive cam in light duty vehicles.

❖ Specific objective

- Modeling of the composite cam using MatLab.
- Simulation for wear of the cam and follower using ABAQUS software 6.10CAE at fixed loading and rpm and pridicting the wear loss values using Archard's Wear Law & Agarwal and Broutmans' law.
- Reinforcement is 4, 3, 2, 1, 10, 4.5 weight % of Nano TiO_2 particle.

1.4 Organization of the paper

This thesis is organized in to five chapters. In the first chapter, background and justification of this thesis work, introduction of different terms, objectives to be achieved and statement of the problem to given a solution latter this project are discussed.

In chapter two, a review of literature relevant to this thesis work, which has been investigated by different researchers in relation to this work, is stated.

Chapter three is about the methodology applied, the assumptions considered, analytical methods in modeling of the composite material, and the analytical methods in wear analysis for cam.

In chapter four ABAQUS results of the analysis are summarized and discussions are made based on the outputs.

In chapter five, conclusions based on the result are made. Recommendations are also given. Future works are addressed to researchers.

Chapter two

Literature Review

2.1 Aluminum matrix composites (AMCs)

Electronic books, journals, proceedings, published researches, and others related with current state of the art on reverse logistics where thoroughly reviewed and complied in literature review as part of the research report.

More than 95 articles, books and reports were reviewed focusing on cam failure, wear analysis and composite material from 1990 and 60 of them used in the study as described here bellow.

The selection of the reinforcement particle size influences the strength of the material. The smaller the grain size the better the improvement in the properties [6].

Aluminum matrix composites (AMCs) represent a class of materials that offer a wide range of properties that can measure up with the design requirements of some of the aforementioned applications [7].

AMCs are primarily reinforced with fibers or particulates which are usually ceramic materials (SiC, Al_2O3, WC, B_4C, TiO_2, and BN). They can be produced via solid route processing (such as powder metallurgy) and liquid metallurgy processing routes (rheocasting, compocasting, liquid infiltration, stir casting are a few examples) [8].

[9], In his work produced Al–TiO_2 Nano composites with various amounts of titanium oxide, using powder metallurgy technique. The obtained composites were examined for structural, wear and mechanical properties. Hardness of Al–TiO_2 increases with an increase in the amount of TiO_2 nanoparticles, maximum hardness was 82 BHN and it resulted from the sample containing 4.5 vol. % of TiO_2 nanoparticles. Fig.2.1 shows the effect of TiO_2 particles on the wear rate of Nano composite. It has been found that the weight loss decreased from 1.7 mg to 0.6 mg when the nano TiO_2 particles decreased from 0.5% to 4.5% On the other hand the wear rate of all the investigated samples increased by increasing the applied load.

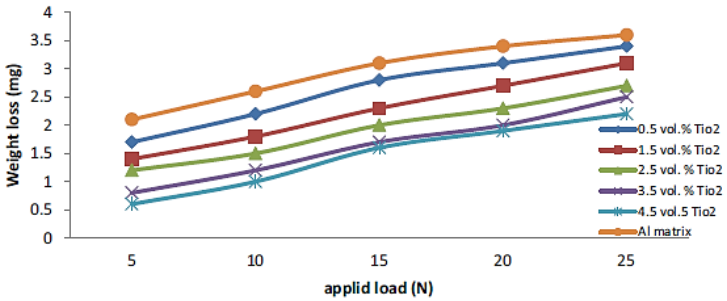

Fig. 2.1 Applied load $V_{s.}$ Weight loss of Al–TiO_2 composites [9]

The stress–strain behavior of all samples has been tested. The figure shows that the ductility decreases with further increase in reinforcement volume fraction. This could be due to the weak bonding between the matrix and the nanoparticles. It is apparent that there are two factors influencing the tensile strength of the composite:

(1) The reinforcing particles increasing the strength of the material by simple load transfer, which depends on the bond integrity at the particle/matrix interface.

(2) The inhibition of plastic relaxation at the particle/matrix interfaces [10].

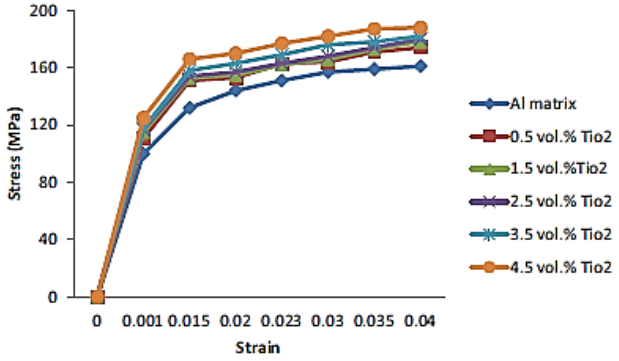

Fig. 2.2 Stress strain relationship in Al–TiO_2 composites [10]

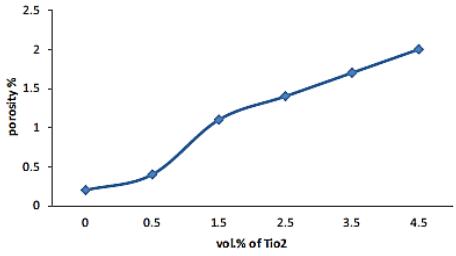

Fig.2.3. Porosity of Al–TiO_2 composites with volume percentage of TiO_2 [10]

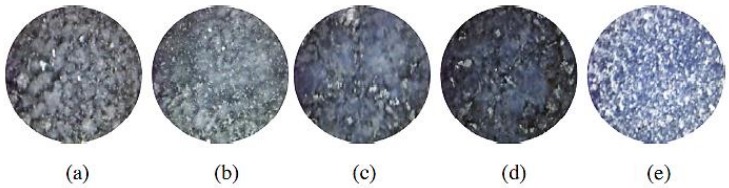

Fig.2.4. Composite microstructure (800x) (a) 0.5% vol. nano TiO_2 (b) 1.5% vol. nano TiO_2 (c) 2.5% vol. nano TiO_2, (d) 3.5% vol. nano TiO_2 and (e) 4.5% vol. nano TiO_2 [10]

[1] Investigated that the tensile test result with the addition of Nano TiO_2 particles to Al matrix composites increases the tensile strength of the alloy at room temperature along with an increase in the TiO_2 particles. The measured maximum and minimum tensile strength of the composite samples were 250 and 198 MPa respectively.

Great enhancement in tensile strength was observed due to the low degree of porosity and the good distribution of Nano ceramic particulates.

[11] Reported that the low degree of porosity results from using powder metallurgy route, which leads to uniform distribution of TiO_2 particles and lower air gaps between grains.

[12] Resulted in his experiment that a significant enhancement in strength is noted initially when the Nano particulate is added; however, the further increase in the amount of TiO_2 nanoparticles leads to a reduction in strength values.

[13] Stated that Hard Nano particles protect the surface of the matrix element, so the wear resistance is enhanced. It was found that the addition of nanoparticles to the matrix alloy increases the hardness; as the Nano TiO_2 particles act as obstacles for the dislocation motion.

[14] In his paper, reported that wear rate decrease with increase in CNT content from 0-1.5 wt% and increase slightly from 1.5 - 2 wt%, then increase rapidly after this range of CNT content. Hardness increases with increase in CNT content from 0-1.5 wt% and decreased gradually from 2.0 wt%.

[1] Reported that TiC particles improved the wear resistance of the AMC. The rate of wear reduced when the volume fraction of TiC particles is increased. TiC particles influenced the wear mode as well as the morphology of the wear debris. The increase in the volume fraction of TiC particles altered the wear mode from adhesion to abrasive.

[13] Also reported that Ti–6Al–4V does provide a significant benefit in terms of its specific strength and stiffness.

[15] in his paper, showed that Cams made of 38–42 HRC chilled cast iron mating with 50–52 HRC chilled cast iron plates after revolutions of 700 p.m., increased the wear of the cam lobe by 9 mm after 56 h and the attack and taper sides by about 12 mm.

[16] Results shows that the Al-micron S_iC Composite Cam were having the almost same wear resistance as the existing Alloy steel Cam. However weight of composites cam was 1/3 of the alloy steel cam.

[13] The particulate reinforced Al-MMCs are easier to recycle than the fiber reinforced composites provided that an appropriate matrix and particulate reinforcement combination is selected.

[4] Overall strength of such particle reinforced MMCs depends on size of the particles, the inter particle spacing, volume fraction of the particles and the nature of matrix and reinforcement interface

[17] Reported that SiC particles were more effective than Al_2O_3 particles for the improvement of wear resistance of Al matrix composites due to their higher hardness. He also reported that SiC reinforced composites have better wear.

[18]Have fabricated Al-SiC Composite valve seat insert with 10, 15, 20 and 25 wt. % of SiC through die compaction of powder and subsequent sintering at 580^oC and compared this composite valve seat insert with steel valve seat insert. It was found that Al-SiC composite valve seat inserts have higher hardness, higher crushing load and good surface finish as compare to steel valve seat inserts and these values were increased by increasing the percentage of SiC with Al alloy up to 10 to 25.

[19] Have fabricated Al -SiC Composite poppet valve guides with 5-30 wt. % of SiC using powder metallurgy as well as stir casting process. The hardness and radial crushing load was measured for the Al-SiC Composite poppet valve guides and were found better than the cast iron poppet valve guides presently used in engine. The hardness, radial crushing load and wear resistance of Al-SiC composite poppet valve guides were found to increase with increase in weight percent of SiC.

Titanium valves are often utilized to reduce weight and so improve performance, their relatively poor wear and corrosion properties at high temperatures [12] make them an expensive proposition

[20] Has studied the wear behavior such as sliding wear, abrasive wear, erosion-corrosion etc. of Al alloy-SiC composite. Attempts have been made to make prototype components out of Al-SiC composites for automobile and mineral processing industries such as brake drum, cylinder block, refrax apex insert etc. which sowed improved wear behaviors.

[21] Studied on Al-SiC composites as a possible alternative material for Cam. A mixture of four different composition (10, 20, 25, 30 wt. %) of SiC powder was prepared and mixed with Al powder. Cams were fabricated using cold isostatic compaction and subsequent sintering. The various properties of fabricated composite cams, namely, compressive strength, hardness, density, and surface roughness were measured and their variation with reinforcement content was studied. The studies showed better properties of the cam.

Many researchers were working on the mechanical properties and dry sliding wear behaviors of aluminum metal composites reinforced with various particulates such as SiC, Al_2O_3, silica sand, boron, TiC, MgO and Si_3N_4 [22]. They observed that the reinforcement material improved the metal yield strength and the ultimate tensile strength.

[6], In his paper has selected Aluminum as matrix alloys for synthesis of AMCs. Fig.2.5 shows the detail drawing of tangential cam with values of different parameters. Base circle radius: 19.5 mm, Nose circle radius: 4.5 mm, Distance between both centre: 24 mm, Total lift: 9 mm, Angle of lift: 150°.

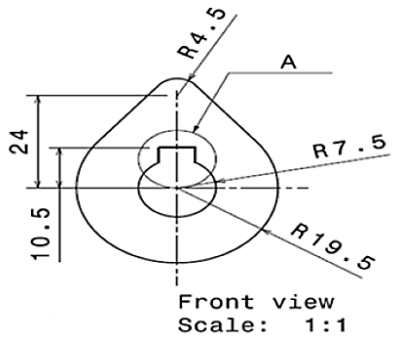

Fig.2.5 Detail Drawing of Cam [6]

The tests were carried out by varying one of the following three parameters at a fixed test time duration of 30 minutes:

(a) Applied load: 10N, 20N, 30N

(b) Sliding Velocity: 0.42 m /s, 0.63 m/s, 0.84 m /s and 1.05 m /s

(c) Sliding distance: 754 m, 1131m, 1508 m and 1885 m.

Conclusions in this paper as shown in Fig.2.6 weight loss in cam at a 2 kg load and 300 rpm for different test durations. Al SiC composite cams with 10 wt. % micron SiC shows lowest wear at the test duration of 2 hours. For all the test durations cam with 10 wt. % micron SiC and existing alloy steel cam show almost same wear. [6]

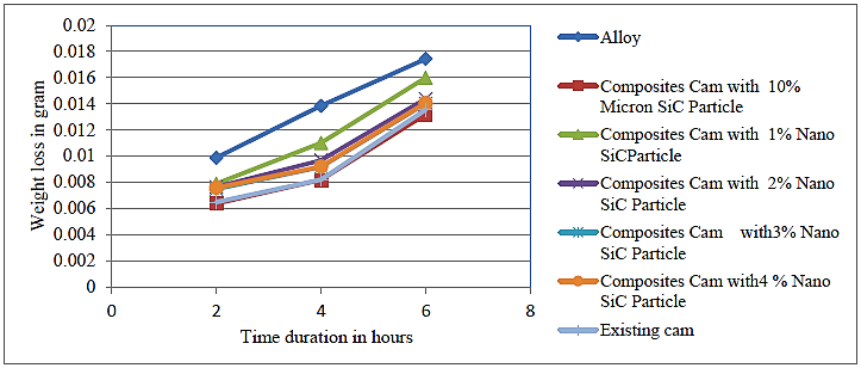

Fig.2.6 Weight loss of cam at load 2 kg and speed 300 RPM [6]

At constant load of 1/2 kg and speed 200 rpm, cam with Al-4 wt. % Nano SiC composites show lowest wear at the test duration of 2 hours. The existing alloy steel cam has shown more wear than Al-4 wt. % Nano SiC composites at 2 and 4 hour test durations.

At a constant load of 2 kg and speed 300 rpm, Al-SiC composite cam with 10 wt. % micron SiC shows lowest wear at the test duration of 2 hours. For all the test durations cam with 10 wt. % micron SiC and existing alloy steel cam show almost same wear.

The wear of existing alloy steel cam and Al-10 % micron SiC composites is almost same.

The Al-SiC composites can be used as alternative material for the cam due to better mechanical properties, lighter weight and similar wear resistance to the existing alloy steel cams. [6]

[23], Made experiment on the cam that test sample is fixed as a pin on cam sample rotating at 90, 100, 110 and 120 rpm. The wear test is conducted under the normal load at 20–85N against AISI 1020 borided steel for adhesive wear. The level variation of cam surface during the wear is

monitored on the computer screen throughout the tests, before and after wear test; the weight loss of the samples is determined.

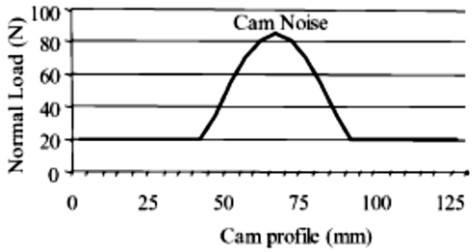

Fig.2.7 The normal load distribution on the cam surface. [23]

[11], Studied the variation of outer coordinates of cam surface due to wear under the load of 20–85N for a 4-h period is shown in Fig. 2.8. The differences between the cam profiles obtained before and after wear test can be seen in Figs. 2.7 and 2.8.

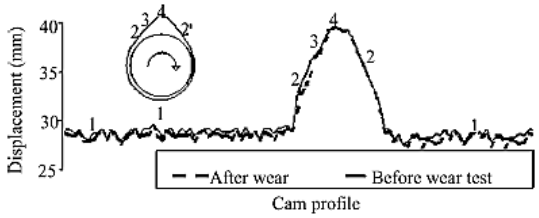

Fig. 2.8 The variation of cam profiles under the adhesive wear conditions. [11]

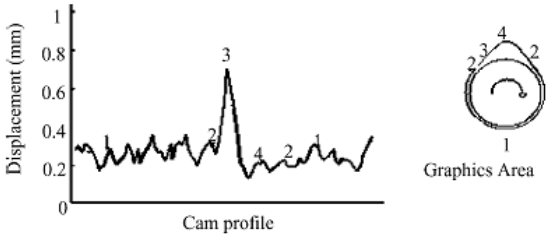

Fig. 2.9. The total height loss of cam according to the reference point on cam under the load of 20–85N for 4 h. [11]

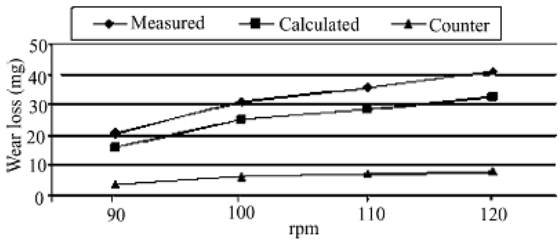

Fig. 2.10. The relations between measured wear and calculated wear value. [11]

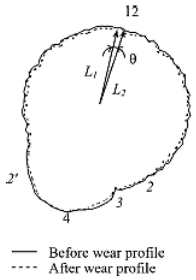

Fig. 2.11 Wear along the cam profile. [11]

After wear test, the trace of adhesion and heavily deformation on the cam sample are given in Fig. 2.11.

[24], in his study divided the cam surface into four sections to analyze wear character of cam surface. Beside these, the height loss of the cam sample is found maximum in section 3. In this section, the wear character is different from the one of the other sections of cam.

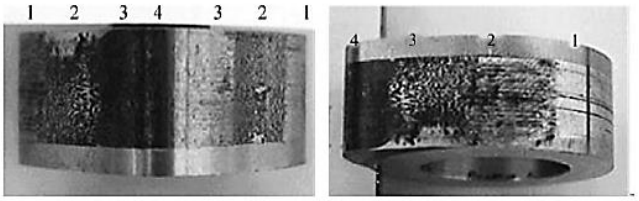

Fig.2.12. The worn cam surface with SEM [25]

[26] Did an experiment and reported as seen from the graphs, it is clear that the brinell hardness number were improved with the addition of titanium dioxide nanoparticles into the aluminum matrix.

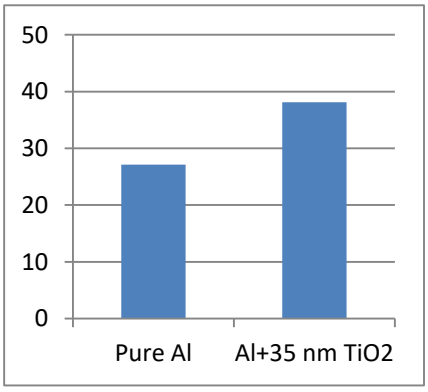

Fig: 2.13 Variation of Brinell hardness number [26]

2.1 Modeling

In order to understand the behavior of systems, mathematical models are required. For this reason, few literatures has been reviewed to find out the best method for this research.

In modeling mechanical properties of Nano composites, there are two main approaches: one is molecular dynamics simulation using direct methods, and the other is finite element simulation using "continuum" methods.

[27]Discussed the method of Molecular dynamics simulation that. It is a technique that allows one to determine the physical and mechanical properties of materials in nanoscale through solving Newton's equations of motion with the atoms interacting through assumed interatomistic potentials. The total potential energy U may consist of a number of bonded and non-bonded interaction terms:

$$U = \sum U_{bond} + \sum U_{angle} + \sum U_{torsion} + \sum U_{inversion} + \sum U_{non-bonded}$$

The first four terms represent bonded interactions, i.e., bond-stretching between two bonded atoms, angle-bending by three neighboring atoms, angle variation between two planes formed by four neighboring atoms, and angle variation of two planes formed by four atoms where one atom is bonded to other three. The last term represents non-bonded interactions between two atoms.

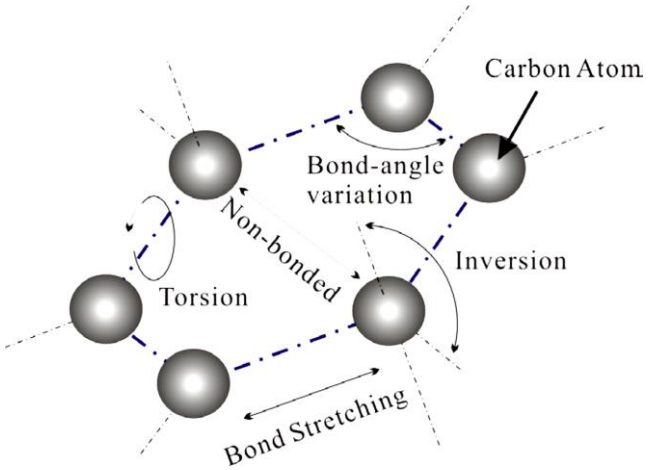

Fig 2.14: Bond structures and corresponding energy terms of a graphene cell. [27]

[28], proposed a new mechanical model for multiphase polymer matrix composites, accounting for size and size distribution effects. It is provided in three structural levels: Nano, micro and macro. The matrix is considered as a micro polar material and the hardening filler nanoparticles.

Multi-steps homogenization procedures are applied to obtain the overall mechanical properties of the composite. This method of homogenization procedure is used in this project.

[2], presented a critical review of the current work of experiment, theory of micro-Nano-mechanics, and numerical analysis on characterizing mechanical properties of Nano composites. First, the classifications of nanomaterial are presented. Then Nano indentation testing and the corresponding finite element modeling, followed by analytical modeling stiffness of Nano composites are presented. The emphasis is on numerical modeling includes molecular dynamics modeling and finite element modeling. Three different approaches are discussed in finite element modeling, i.e. multi scale representative volume element (RVE) modeling, unit cell modeling, and object-oriented modeling are discussed.

In this research multistage homogenization procedure is used through MatLab.

2.2 Wear analysis & simulation

[29], In his paper used experimental method to study characterization of cam and follower wear. The running is investigated by analyzing the change in topography of the roller, pin and rocker arm of the fuel injector arm.

[30], Investigated the characteristics of an engine cam and follower system including contact pressure, surface wear, and the effect of contact pressure on surface wear of cam and follower system. To estimate the effect of contact pressure the characteristics of cam and follower system were analyzed by using the finite element method. He also summarized sum simulations in order to define an acceptable model to run 3D finite elements analysis and calculated the contact pressure.

[31], used experimental method to investigate the characterization of wear on a cam follower system in diesel engine. The investigation focused on the effect of cam and follower materials and their thermal and thermo-chemical treatment on cam and follower functional properties. During the investigation the preferred material for cam shaft mating with a slide cam follower is gray metallurgical hardened cast iron. And the mating follower made of chilled cast iron, hardened and tempered.

[32], Studied the contact stress analysis of cam and follower using finite element analysis. He determined the stress concentration on the cam and follower during normal operation. The finite

element analyses are done for determination of stress concentration during 30 degree of cam and during maximum exhaust valve lift.

[5], Investigated an impact model for the industrial cam- follower system using simulation and experiment. From this model, an insight into proper design of systems with deliberate impact was developed through computer modeling. To attain more precise representation on a simplified industrial cam – follower system model was constructed in Solid Works CAD software.

[13] Apart from the classical approach, the software AVLTYCON is used to generate the cam profile, the kinematic and dynamic analysis of valve train system. The relative velocities, acceleration, radius of curvature of the cam and follower contact stress are accurately predicted using this tool.

Investigation has also been focused on the wear behavior of aluminum metal matrix composite (MMCs) reinforced with different composition (5%, 10% and 15% by weight of aluminum) of titanium dioxide (TiO_2) and stir casting is used to produce this composite. Dry and abrasion test and sliding wear test was performed on the MMCs.

In this reasurch wear analysis will be made through Archard's wear law and the wear will also so simulated using ABAQUS.

2.3 Manufacturing methods

There are different manufacturing techniques for reinforcing alloy such as spray decomposition, liquid metal infiltration, powder metallurgy, squeeze casting, mechanical alloying and compo casting [33] [34] [35].

Powder Metallurgy (PM) is a highly-developed technique for manufacturing composites; this technology consists of three steps; mixing powder elements, compacting those powder elements in a die at room temperature and then heating in a controlled atmosphere furnace to create a bond between the powder elements [36].

Without disregard to the technical competence of other processing routes available, stir-casting remains the most utilized technique due to its simplicity, flexibility, low cost acquiescence and commercial viability [37].

[38] Described in his paper that Boron Carbide (B_4C) composites_incorporated with 5 wt. % of boron carbide particles with an average size 33μm was fabricated through stir casting process.

Currently, there are several fabrication methods of MMCs and MMNCs, including mechanical alloying with high energy ball milling, Stir casting process, disintegrated melt deposition, powder metallurgy, ultrasonic assisted casting etc. [16]

In this research manufacturing of the material will not be made, however, it's concluded from different researches that the best method for manufacturing of the composite cam is powder metallurgy due to its best dispersion of the nano materials.

Chapter Three

Analytical Methods and Materials

3.1 Material

The preferred material for a cam mating with slide cam follower at direct valve drive is aluminum Nano composite material with Aluminum alloy 5083 as the matrix element and 4% TiO_2 as Nano particle. Aluminum alloy has the following chemical composition: 4.00 – 4.90% Magnesium (Mg), 0.40 – 1.00% Manganese (Mn), 0.40 % Typical Iron (Fe), 0.0 – 0.40 % Silicon (Si), 0.05 -0.25% Chromium (Cr), 0.10 % Typical Copper (Cu), 0.0 – 0.15 % Others (Total), 0.0 – 0.10 Zinc (Zn), 0.0 – 0.05% Other (Each), and Balanced Aluminum. The minimum hardness of cam should be 82BHN. The mating valve has minimum hardness of 64BHN.

3.2 Engine Cam wear analysis dimensions

Wear modeling and simulation is going to be carried away using ABAQUS software 6.10CAE for composites with Al5083 alloy and 4%, 3%, 2%, 1%, 10%, 4.5% of Nano TiO_2. The test is going to be carried away by the indicated parameters at a fixed test time duration of 6 hours.

3.3 Assumptions

- The model doesn't consider overlapping of interphase zones.
- Equal particle size is considered
- Equal distribution of Nano particles
- Interface effect is ignored for metal matrix composite. (Nano and the metal matrix property only)

3.4 Conditions

Dimension: Base circle radius: 19.5 mm, Nose circle radius: 4.5 mm, Distance between both Centers: 24 mm, Total lift: 9 mm, Angle of lift: 150°.

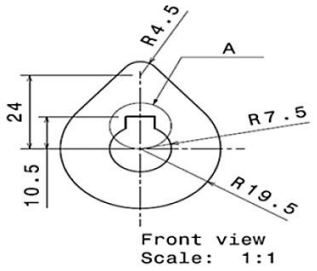

Fig 3.1 Cam dimensions [6]

Load range: Constant load of 2 Kg is going to be applied.

Force: Applied load: 20N

Pressure: Maximum contact pressure is 1025.15Mpa at the cam lobe.

Temperature range: room temperature for low rpm of 300.

Speed: 300rpm

Weight percent of Nano TiO_2: 4%, 3%, 2%, 1%, 10%, 4.5%

Follower type: Round faced follower;

Valve/ Port design and location: I head single overhead cam (SOHC)

3.5 Analytical Methods in modeling of the composite cam

Particulate Nano-composites are composite materials based on matrix material which is reinforced by one or more Nano materials in order to improve their performance properties. New technologies use methods leading to composites in which the fillers are specifically aligned or nearly homogeneously dispersed. The most common matrix materials are polymers, ceramics and metals.

- Modeling

The modeling is carried out on three levels. At Nano level the composite consists of three phases: matrix, nanoparticles and interphase zone around the particles, considered as additional phase. The properties of this transition zone are not constant and vary from the properties of the inclusion at the inner boundary to the properties of the matrix at the outer boundary. The transition from Nano to micro level is realized over a homogenization procedure. It transforms the Nano inclusion and its surrounding interphase area into a single homogeneous particle with new properties, accounted further on micro level. At micro level the material considered is a multiphase particle reinforced composite with size sensitive matrix. At this level a two-step homogenization procedure is realized. At macro level we deal with an isotropic Cauchy type mono-phase material obtained after homogenization. The consecutive stages of homogenization from Nano to macro level are presented schematically.

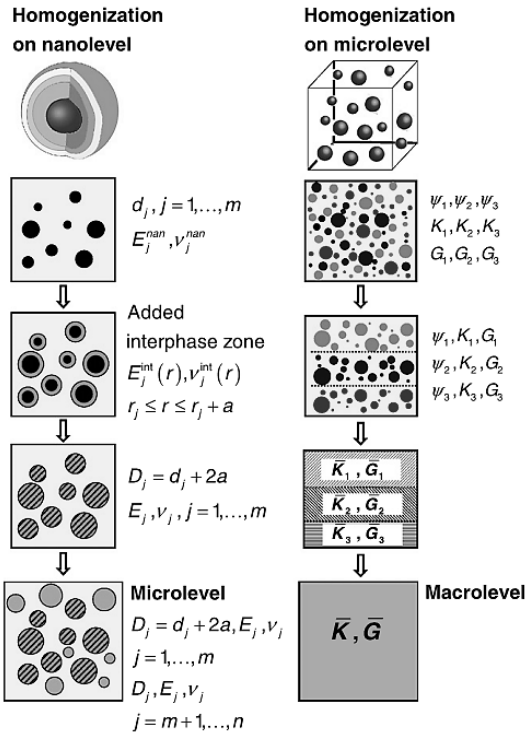

Fig. 3.2: Scheme of multi scale homogenization procedures for multiphase composite [39]

- ✓ Modeling at Nano level

Let the composite contain m different spherical Nano phases with corresponding diameters dj = 2rj, with j =1, ... , m. As the inclusions are much harder compared to the matrix, they are assumed pure elastic with Young's modulus E_j^{nano} and Poisson's ratioν_j^{nano}. The shear and the bulk modulus of the Nano inclusion are:

$$G_j^{nan} = \frac{E_j^{nan}}{2(1+\nu_j^{nan})} \quad \text{.....(3.01)}$$

$$K_j^{nan} = \frac{E_j^{nan}}{3(1-\nu_j^{nan})} \quad \text{.....(3.02)}$$

The transition zone around each particle is assumed of nano size which can be generally functioning of the matrix and of the inclusions properties. The properties of this transition zone are influenced strongly on the particle properties. The model does not consider overlapping of interphase zones. We assume that the properties in the interphase region are defined with:

$$E^{(j)}(r) = E_{min} + (E_{max} - E_{min})\left(\frac{r_j + a - r}{a}\right)^{\beta_g} \quad \text{.....(3.03)}$$

$$\nu^{(j)}(r) = \nu_o,\ r_j \le r \le r_j + a \quad \text{.....(3.04)}$$

Generally, the values of E_{min}, E_{max} and $\beta_g > 0$ depend on the contact conditions between inclusions and matrix. Their proper choice enables some particular features of the manufacturing process, as surface treatment of the fillers before mixing, existence of filler coating, etc. to be taken into account.

For example two fillers with equal mechanical properties and size distribution but with different adhesion to the matrix would lead through these parameters to different interphase properties and hence to different properties of the overall composite.

In the case of coating $\beta_g \ll 1$ and E_{max} corresponds to the coating Young's modulus. a is then equal to the coating thickness.

The case $\beta_g = 1$ corresponds to a linear transition of the properties from E_{max} toE_{min}.

In this case of we assume that $E_{min} = E_o$ and$E_{max} = E_j^{nano}$.

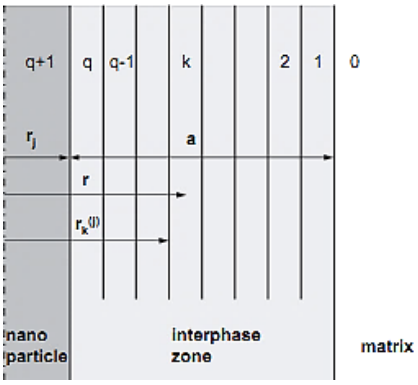

Fig. 3.3: Scheme of interphase zone around the inclusion. [39]

The parameter β_g enables the physical–chemical interaction between fillers and matrix to be taken into account.

$$\beta_g = 1 + \frac{d_{mean}^2}{2a(L)} \quad \text{.....} \quad (3.05)$$

Where $d_{mean}$the averaged diameter of particles and L is the averaged surface to surface inter particle distance.

The range of influence of nanoparticles (the thickness of the interphase zone) is equal to the radius of gyration R_g.

$$a = R_g \text{ If } (L) \geq 2R_g \quad \text{.....} \quad (3.06)$$

$$a = \frac{1}{2}(L) \text{ If } (L) \leq 2R_g \quad \text{(3.07)}$$

$$\langle L \rangle = d_{mean}\left[\left(\frac{C_{summax}}{C_{filler}}\right)^{1/3} - 1\right] \quad \text{(3.08)}$$

If the interface region is divided into q concentric subareas, the discrete version of the above relation will be rearranged to the following;

$$E_k^{(j)} = E_o + (E_j^{nan} - E_o)\left(\frac{r_j + a - r_k^{(j)}}{a}\right)^{\beta_g} \quad \text{(3.09)}$$

$$r_k^{(j)} = r_j + a\left(1 - \frac{k-1}{q}\right) \quad \text{(3.10)}$$

$$v_k^{(j)} = v_o, k = 1, \dots, q \quad \text{(3.11)}$$

$$C_k^{(j)} = \frac{(r_j + a\frac{q-k+1}{q})^3 - (r_j + a\frac{q-k}{q})^3}{(r_j + a)^3}, k = 1, \dots, q \quad \text{(3.12)}$$

$$C_{q+1}^{(j)} = \left(\frac{r_j}{r_j + a}\right)^3$$

- ✓ 3.5.1.2 Modeling at Micro level

Modeling of the hardening phases

The hardening particles at this level are assumed elastic spheres with different diameters and mechanical properties. They can be grouped in a finite number n > 2 of sets, according to the diameters D_i, (i =1, ..., m, m +1, ... , n). The first m sets are the result of the homogenization procedure at nanolevel. The volume fraction of each set is Ci. The total volume fraction of the hardening phases (equivalent inclusions) is,

$$C_{sum} = \sum_{i=1}^{n} C_i = C_{nano} + C_{intphs} + C_{micro} \quad \text{(3.13)}$$

Where $C_{nano}$is the total volume fraction of the Nano size filler, C_{intphs} is the total volume fraction of their interphases and C_{micro} is the total volume fraction of the micro scale fillers.

Modeling of the matrix material

$$K_o = \lambda_o + \frac{2}{3}\mu_o \quad \text{(3.14)}$$

$$N = \alpha + \frac{2}{3}\beta \quad \text{(3.15)}$$

Where $\lambda_o = \frac{E_o v_o}{[(1+v_o)(1-2v_o)]}$, μ_o are the elastic Lamé constants, a, b, c and j are the Cosserat material constants. K_o and N are Cauchy and Cosserat bulk moduli respectively, E_0 is Young's modulus and v_0 is Poisson's ratio. $G_0 = \mu_o$ is Cauchy shear modulus.

$$K_{ci} = K_o\left[1 + \frac{C_{sum}(K_i - K_o)}{C_o a_o (K_i - K_o) + K_o}\right] \quad \text{(3.16)}$$

$$G_{ci} = G_o\left[1 + \frac{C_{sum}(G_i - G_o)}{C_o b_{oi} (G_i - G_o) + G_o}\right] \quad \text{(3.17)}$$

The following notations are used in the above formulas,

$$a_o = \frac{3K_o}{3K_o + 4G_o}, b_{oi} = \frac{6(K_o + 2G_o)}{5(3K_o + 4G_o)} - \frac{6k}{5(k + G_o)} R_i(\eta_i), \quad \text{(3.18, 19)}$$

If the matrix is considered as a classical Cauchy material (k = 0), the second term in the expression for b_{0i} vanishes.

Modeling at macrolevel

$$K_c(D) = K_o\left[1 + \frac{(1 - C_o)(K_{inc} - K_o)}{C_o a_o (K_{inc} - K_o) + K_o}\right] \quad \text{(3.20)}$$

$$G_c(D) = G_o\left[1 + \frac{(1 - C_o)(G_{inc} - G_o)}{C_o b_o(D)(G_{inc} - G_o) + G_o}\right] \quad \text{(3.21)}$$

And,

$$\int_0^\infty \frac{\Psi(D)}{1 - \frac{3K_o}{3K_o + 4G_o\left(1 - \frac{K_c(D)}{K_o}\right)}} dD - 1 = 0 \quad \text{(3.22)}$$

$$\int_0^\infty \frac{\Psi(D)}{1 - \frac{2(3K_o + 6G_o)}{5(3K_o + 4G_o)\left(1 - \frac{G_c(D)}{G_o}\right)}} dD - 1 = 0 \quad \text{(3.23)}$$

$\Psi(D)$ Is density distribution function

3.6 Density of a Nano composite material

The theoretical density of composite materials in terms of weight fraction can easily be obtained as for the following equations given by Agarwal and Broutman. [40]

$$\rho_c = \frac{1}{\frac{W_m}{\rho_m} + \frac{W_p}{\rho_p}} \quad \text{(3.24)}$$

Where ρ_c is density if the composite.

Wm is weight of the matrix material.

Wp is weight of the Nano particle.

ρ_m Is density of the matrix material.

ρ_p Is density of the Nano particle.

3.7 Wear Modeling

Mechanical wear on cam and follower valve contacts has different parts that are damaged by different types of wear such as abrasive wear, adhesive wear, plastic deformation and fatigue wear. These parts are the valve, cam lobe, basic surface and cam flank. Wear on this parts occur depending on the contact pressure, pressure angle and cam angle.

Most common wear model is Archard's Wear Law expressed as follows;

$$V = k * \frac{F_n}{H} * S \quad \text{..... (3.25)}$$

Where V is the wear volume,

K is wear coefficient,

S is sliding distance,

H is the hardness, and

F_n is the normal force

The wear volume per sliding can also be expressed by;

$$Q = \frac{K * F_n}{H} \quad \text{..... (3.26)}$$

Brinell hardness number is predicted by indenting the composite material a 10mm diameter hardened steel ball. Applied loads can be 500Kg for soft material, copper, brass, thin stock; 1500kg for aluminum casting and 3000kg for iron and steel for a time duration 10 to 15sec.

$$BHN = \frac{F}{\frac{\pi}{2}D.(D-\sqrt{D^2-D_i{}^2}} \quad \text{..... (3.27)}$$

Where BHN is Brinell hardness number

F is applied load

D is indenter diameter

D_i is indentation diameter, can be calculated as,

$$D_i = \frac{D^2 * 3014159}{2}. \quad \text{(3.28)}$$

In this research, hardness for composites of aluminum until 4.5wt% of TiO_2 is taken from hardness test made from past resources as shown in the figure bellow. It can be seen that the hardness of Al–TiO_2 increases with an increase in the amount of TiO_2 nanoparticles, this may be due to nanoparticles, which hindered the movement of matrix dislocation in the composite leading to increased strength and hardness.

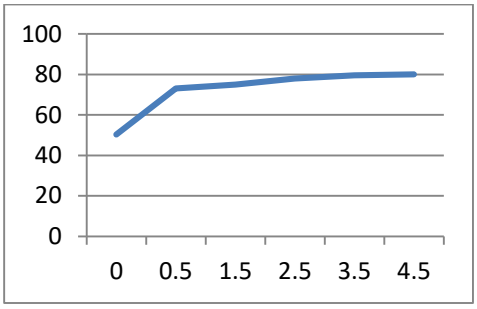

Fig. 3.4: Hardness of Al–TiO_2 composite material with different weight percentage of TiO_2

3.8 Analytical Methods in wear analysis of cam

- Wear on cam lobe

The cam lobe, which is at an angle from 147 – 180 and from 180 – 212 angle of cam is characterized by widest wear track since this area is exposed to high load due to extremely compressed follower valve spring producing high pressure, high temperature and high sliding - rolling action resulting in plastic deformation, abrasion and sever scratch.

Wear by Plastic Deformation

This type of deformation occurs due to applied high load on small area resulting in high temperature and pressure. It can be verified by calculating the total deformation of the contacting bodies according to Hertz theory.

$\delta = \frac{b^2}{R}$, ……...…… (3.29)

where b is half contact width and R is radius of curvature.

Wear by Abrasion

Wear volume caused by abrasive wear is calculated by the following formula.

$V = \frac{\alpha\beta * F_n * s}{H}$, ……..……...…… (3.30)

where F_n load, s is sliding distance expressed by dS = X*dθ; X being a distance from center of cam to the point of contact. α is the shape factor of an asperity, 0.1. β which varies between 0 and 1.0 depending on the value of the degree of penetration of an abrasive asperity, the shear strength at the contact interface and mechanical properties of the wearing material, is the degree of wear by abrasive asperity. H is the hardness.

Wear rate can also be expressed by specific wear rate,

$W_s = \frac{\alpha\beta}{H}$ ……...…… (3.31)

Or wear coefficient, K =αβ ……..……...…… (3.32)

Or by a function of sliding velocity $V = k * p * v_s * t$ ……...…… (3.33)

Where p is contact pressure, v_s is sliding velocity.

This sliding velocity is the part of tangential velocity at the contact point. $V_t = X\dot{\theta}cam$.

$D(\theta) = r_b + u(\theta)$ ……...……..…… (3.34)

$u(\theta) = 0.5h(1 - \cos\pi\frac{\theta}{\theta_A})$, for raising action of the follower; ……...……..…… (3.35)

And, $(\theta) = 0.5h(1 - \cos\pi\frac{\theta - \theta_c}{\theta_b - \theta_c}$, for returning action. ……...…… (3.36)

Where θ = cam angle, $\theta_b, \theta_a, \theta_c$ are transition points. $\dot{\theta}_{cam}$ is rotational speed of cam. Then sliding velocity is expressed as $V_s = v_t \cos\alpha$. α here is the pressure angle.

V becomes, $V = k * p * x\dot{\theta}_{cam}\cos\alpha\alpha * t$……..…….…… (3.37)

Then wear for the rising action follower being in contact with the cam from 147^0 to 180^0 is $V = k * p * \left(rb * 0.5h\left(1 - \cos\pi\frac{\theta}{\theta_A}\right)\right)\dot{\theta}_{cam}\cos\alpha * t$

While wear for returning action is $V = k * p * \left(rb * 0.5h\left(1 - \cos\pi\frac{\theta-\theta_c}{\theta_b-\theta_c}\right)\right)\dot{\theta}_{cam}\cos\alpha * t$

Pressure, distance between center of cam and contact point, and cosine value of pressure angle when the pressure angle is 180^0 results sever wear at the top of the cam lob, expressed by $V = k * p_{max} * x_{max}\dot{\theta}_{cam}\cos\emptyset * t$

Instantaneous rate of wear $i(x,t) = k * p * h * G * V_s$. Where G is semi elliptical pressure distribution.

Finally the wear occurring during a single passage of contact of cam surface is given by bellow formula where t_1 and t_2 are the time at the start and end of contact point on cam surface.

- Wear on basic circle surface

In this analysis, the wear coefficient, radius of basic circle and hardness are constants. Angular speed is 200rpm.

Wear rate at the cam basic circle surface is directly proportional to the normal force, expressed by, $V = \frac{K*F_n*s}{H}$.

Where sliding distance $ds = r * d\theta$ and $\theta = \omega * t$.

Rate of wear is expressed by $Q = \frac{K*F_n*r\omega t}{H}$

θ is angular position of cam and r is basic circle radius.

Pressure angle at the basic circle surfaces is constant throughout and the pressure angle is 0^0. Spring force is small and contact area is high resulting low wear rate (volume) and negligible plastic deformation due to low pressure and temperature at the surface.

❖ Wear on cam flank

Flat surface cam flank, from 82^0 to 147^0 of cam rotational angle is exposed for sliding and rolling action and more of sliding contact.

This sliding contact causes different types of wear mechanisms such as pitting, scuffing, and scoring.

Archard's law stays at the basis of different types of wear mechanisms and proposes relation between the rate of wear, contact pressure and rate of slippage.

$\frac{\partial w}{\partial t} = kpv$……..…….…… (3.38)

$v = \frac{\partial s}{\partial t}$……...……...…… (3.39)

And $w = \int_{s1}^{s2} kp\,\partial s$ generalized as $w = kps$…….....…… (3.40)

Where k is wear coefficient, p is contact pressure, v is wear rate and s is slippage. For the raising action of the valve train system, wear rate increases with increase of cam rotational angle. Here, the wear equation can be expressed by;

$w = k * \frac{F_n}{H} * s$

3.9 Analytical Method in wear displacement of the cam

Wear displacement is directly proportional to contact pressure and inversely proportional to hardness of the material as shown below. First, let us consider h as the wear depth, A as the contact area, and V as the wear volume.

$V = hA$……..…… (3.41)

$V = k\frac{F_n}{Hs}$

$h = k\ \frac{F_n}{HsA}$ Where $\frac{F_n}{A}$ is pressure, p.

Then the wear displacement becomes $\frac{dh}{ds} = k\frac{P}{H}$ with respect to infinitesimal sliding displacement.

The sliding distance as shown below can be expressed as follows. First, let us consider cam radius of R. The follower and cam are pressed together by force, F_n and cam rotates at angular velocity of ω. Wear of the contacting surfaces is $v = \omega . R$.

The wear of the contact surfaces is described by the following wear model;

$$\frac{dh_i}{dt} = k_i * p * V_{i,s} \quad \text{(3.42)}$$

Where $i = 1$ for cam and $i = 2$ for follower valve. h_i is the wear depth at a point on surface I when it rubs against the opposite contact surface, k_i is the wear coefficient for point on surface i when it rubs against the opposite contact surface, p is the local contact pressure, and $V_{i,s} = v_1 - v_2$ for points on both contact surfaces is the sliding velocity at a point on surface i sliding against the opposite interacting surface.

Therefore, for the starting action, $\int_0^{h_i} dh_i = \int_0^t (K_i * p * (v_1 - v_2))d_t$ (3.43)

Wear of the next duration, $\int_{hi,old}^{h_{i,new}} dh_i = \int_{t_1}^{t_2} (K_i * p * (v_1 - v_2))d_t$ (3.44)

The integral equation can also be formulated as follows,

$h_{i,new} = h_{i,old} + \int_{t_1}^{t_2} (K_i * p * (v_1 - v_2))d_t$, where$V_{i,s} = \omega * R$; ω is angular velocity of cam and R is radius of curvature. Reformulating the above formula gives

$$h_{i,new} = h_{i,old} + \int_{t_1}^{t_2} (K_i * p * \omega * R)d_t$$

From the above equation K_i and R are constants. $\omega * d_t$ is the infinitesimal angular position of the rotating cam.

Thus using the method below, one can describe the wear displacement value in terms of cam angle.

$$h_{i,new} = h_{i,old} + k_i * R \int_{\theta_1}^{\theta_2} P d\theta \quad \text{(3.45)}$$

Chapter Four

Result and Discussion

4.1 Result

In this section results from finite element method i.e. the results using abaqus for contact stress and the theoretical analysis with the application of hertz contact theory for stress analysis will be described and the results will be compared.

The finite element representation of cam and follower systems have three position the at the follower will in contact with the cam surfaces. These are the cam basic surface, the cam flank and the cam lobe. The results of these three conditions are depicted.

This section of the research also shows the abaqus wear analysis simulation results made by using the properties found by using the MATLab software at 4.5% ,4%, 3%, 2%, 1%, 10% weight of Nano titanium dioxide. Results of weight loss will be compared to same percentage contents of Nano SiC- Al cam (i.e) 4% weight of Nano SiC and TiO_2.

Analytical results of the cam wear loose are found to be 0.0055 minimum at 4.5 wt% TiO_2 and maximum 0.008 maximum in grams at 10 wt% TiO_2. At 4 wt% TiO2 wear loose value is found to be 0.006 grams.

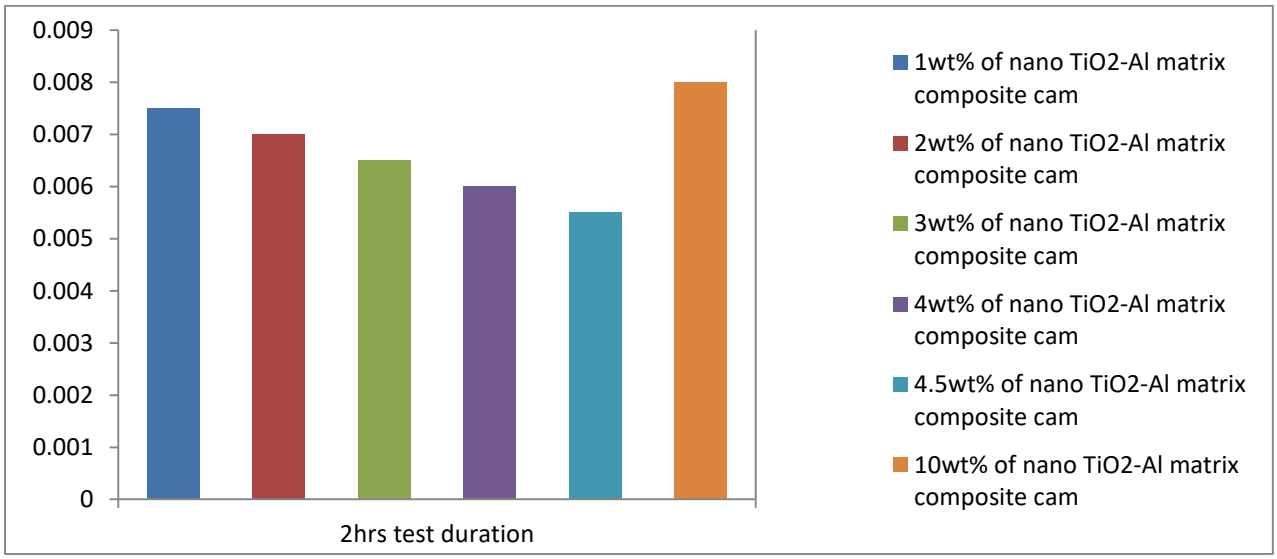

Fig. 4.1 Wear loose of Al-TiO_2 composite cam at different weight present and fixed time duration

❖ ABAQUS simulation at weight present of 4% Nano TiO_2-Al Cam

Cam Basic Circle

The figure bellow shows the contour plot of distribution of von misses stress along the cam basic circle surfaces when the roller is in contact with the cam basic circle surface.

Numerical value of the von misses stress resulted from Abaqus is maximum: +4.832e-02MPa which is less than the yield strength of the composite predicted using the homogenization approach.

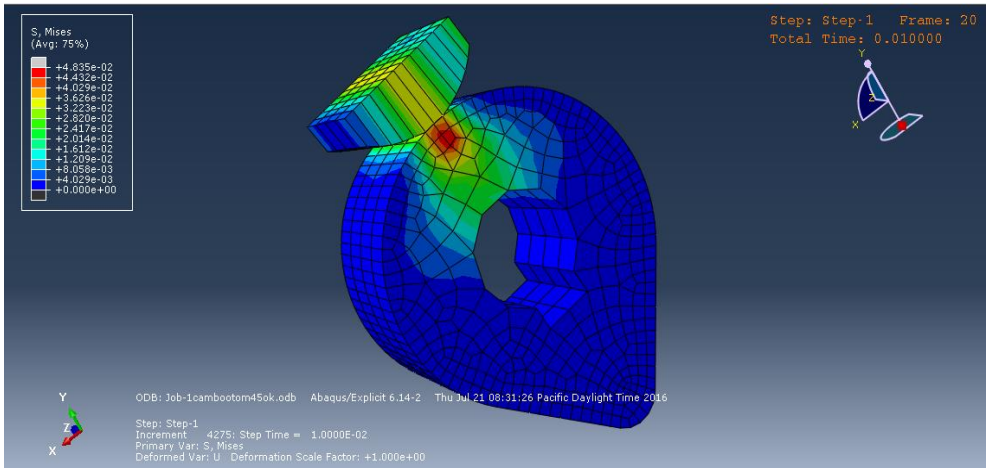

Fig 4.2 Distribution of von misses stress at the cam basic circle

Numerical value of the contact pressure resulted from abaqus is maximum: +9.328e-02MPa.

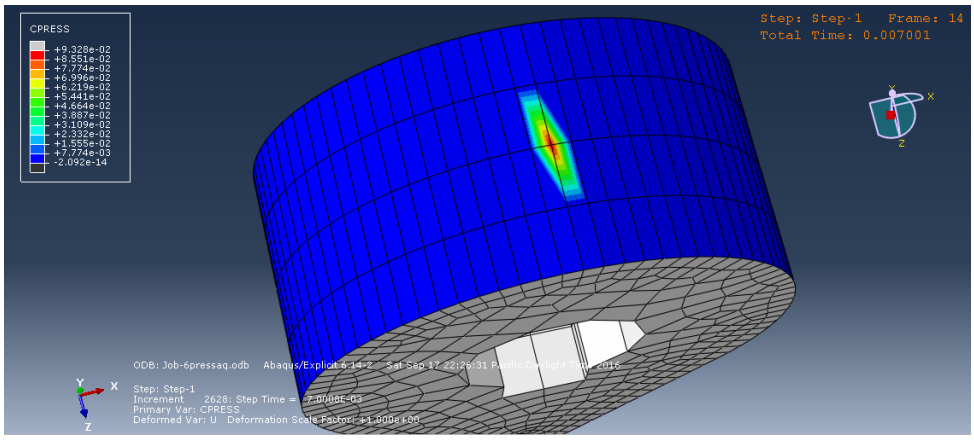

Fig 4.3 Distribution of contact stress at the cam basic circle

Cam Flank

The figure bellow shows the contour plot of distribution of von misses stress along the cam flank surface when the roller is in contact with the cam flank surface.

Numerical value of the von misses stress resulted from abaqus is maximum: +4.369e-02MPa.

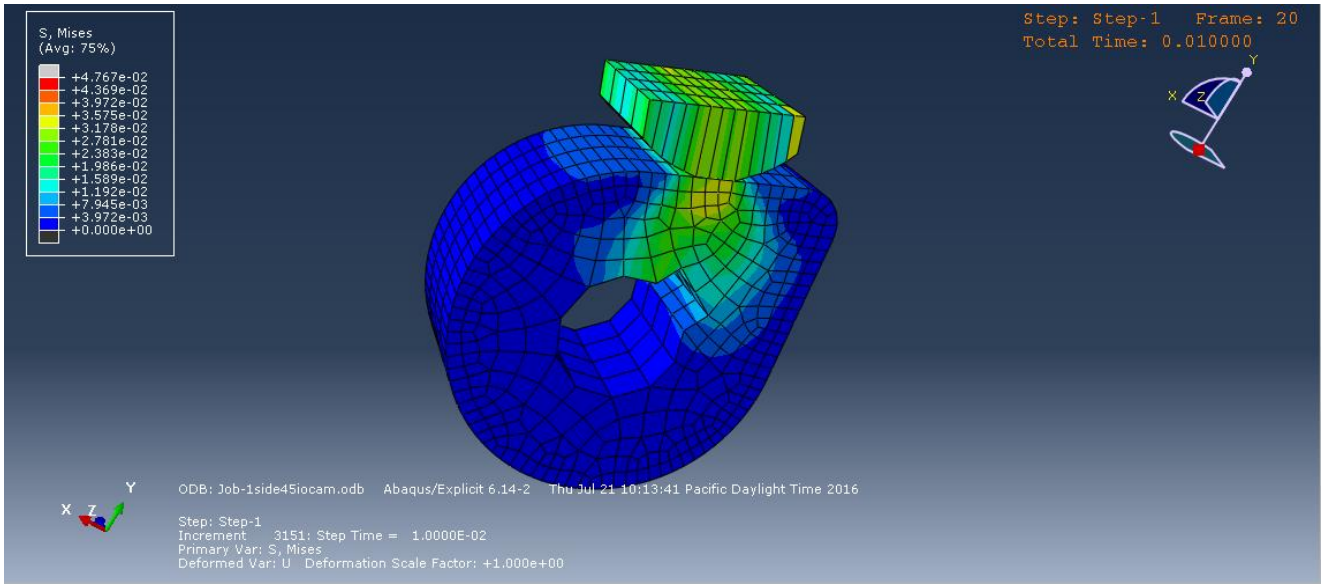

Fig 4.4 Distribution of von misses stress at the cam flank

Numerical value of the contact pressure resulted from abaqus is maximum: +5.553e-01MPa.

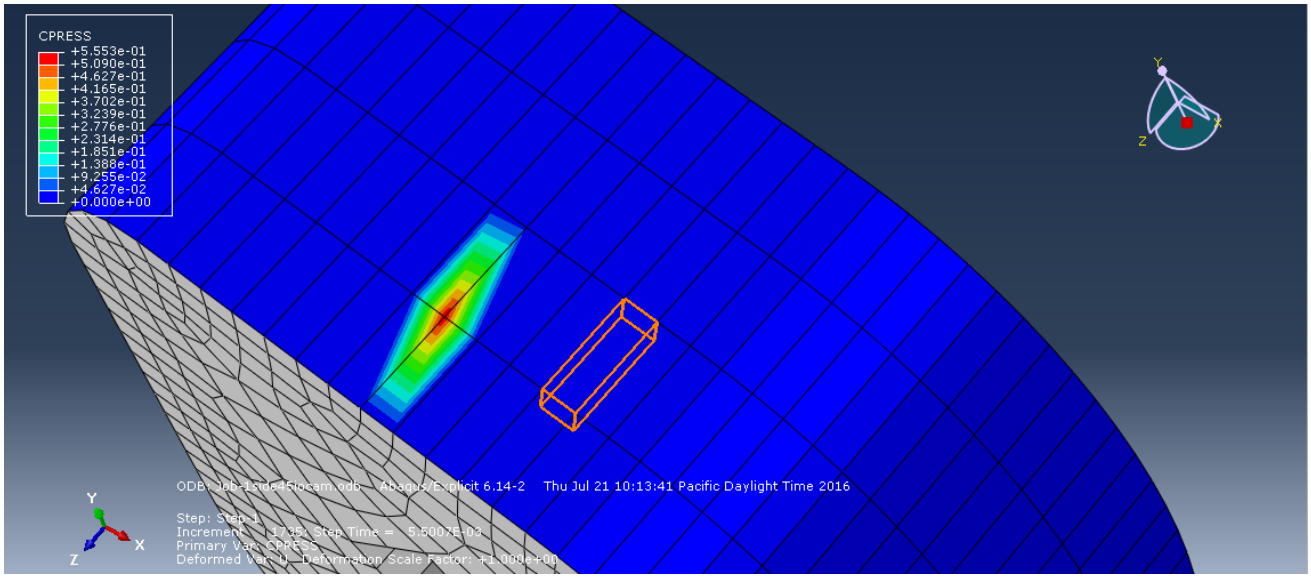

Fig 4.5 Distribution of contact stress at the cam flank

Cam lobe

The figure bellow shows the contour plot of distribution of von misses stress along the cam flank surface when the roller is in contact with the cam lobe surface.

Numerical value of the von misses stress resulted from abaqus is maximum: +5.040e-02 MPa which is acceptable for this specific material.

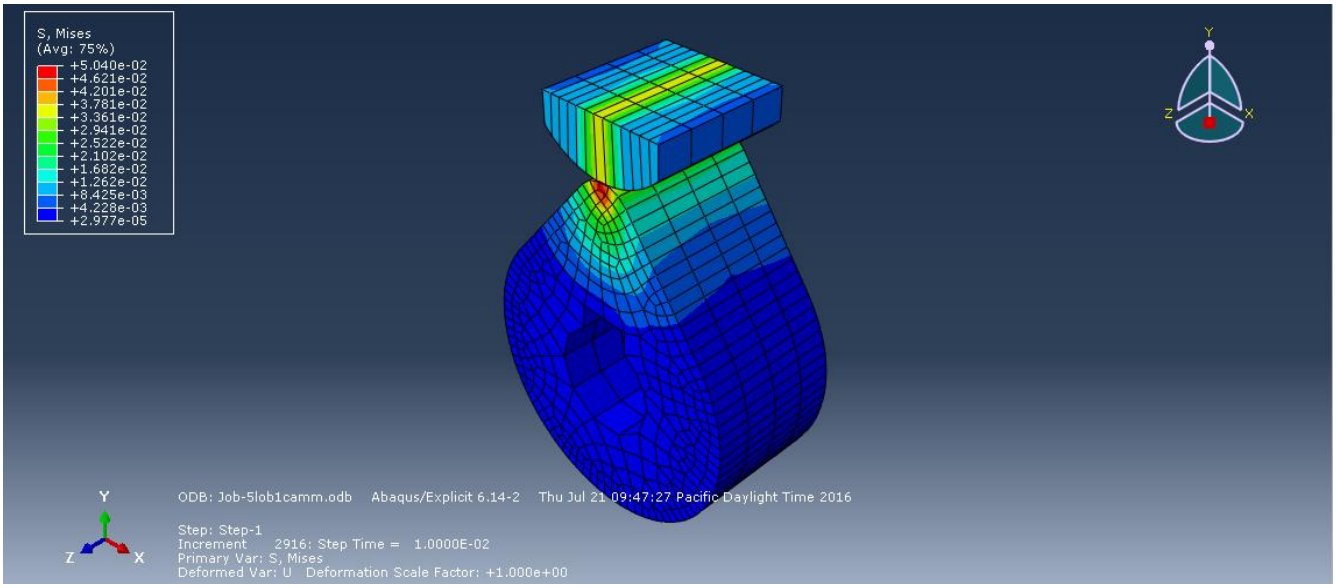

Fig 4.6 Distribution of von misses stress at the cam lobe

Numerical value of the contact pressure resulted from abaqus is maximum: +2.226e-01MPa.

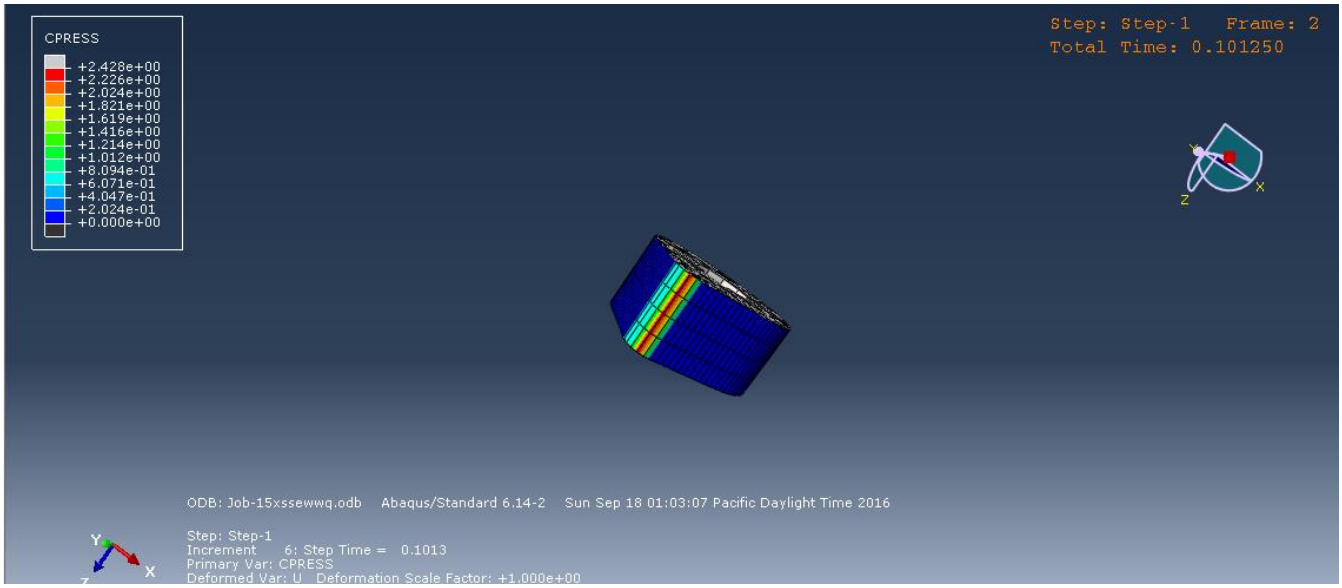

Fig 4.7 Distribution of contact stress at the cam lobe

- ABAQUS simulation at weight present of 3% Nano TiO_2-Al Cam

Cam Basic Circle

The figure bellow shows the contour plot of distribution of von misses stress along the cam basic circle surfaces when the roller is in contact with the cam basic circle surface.

Numerical value of the von misses stress resulted from abaqus is maximum: +4.771e-02MPa and again acceptable for this specific material.

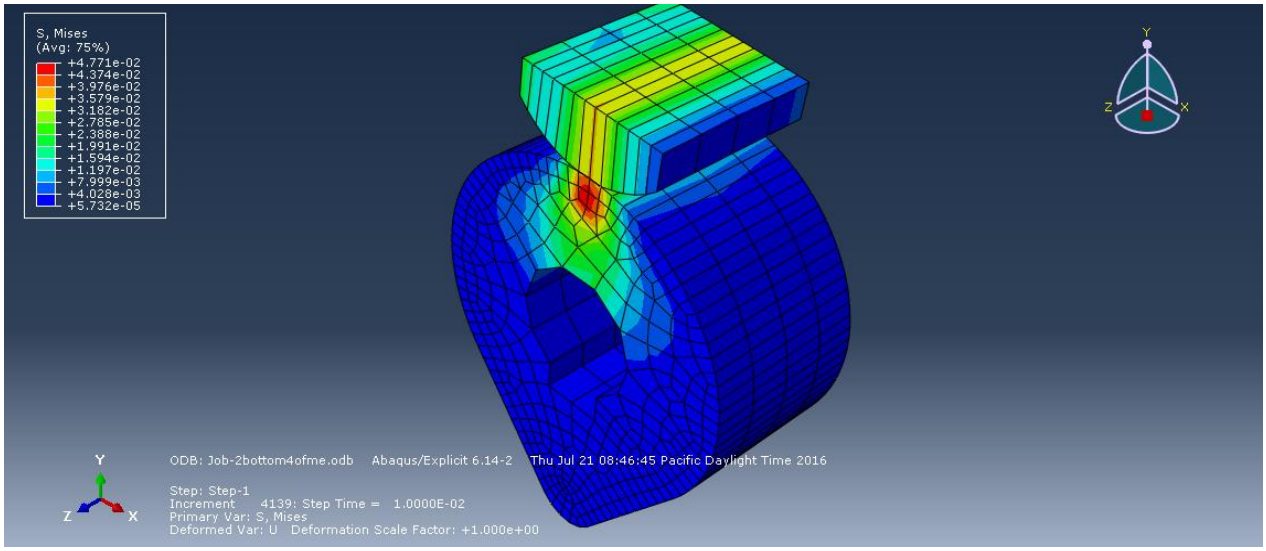

Fig 4.8 Distribution of von misses stress at the cam basic circle

Numerical value of the contact pressure resulted from abaqus is maximum: +9.354e-02MPa.

Cam Flank

The figure bellow shows the contour plot of distribution of von misses stress along the cam flank surface when the roller is in contact with the cam flank surface.

Numerical value of the von misses stress resulted from abaqus is maximum: +4.587e-02MPa also within the safe range for the material loading capacity.

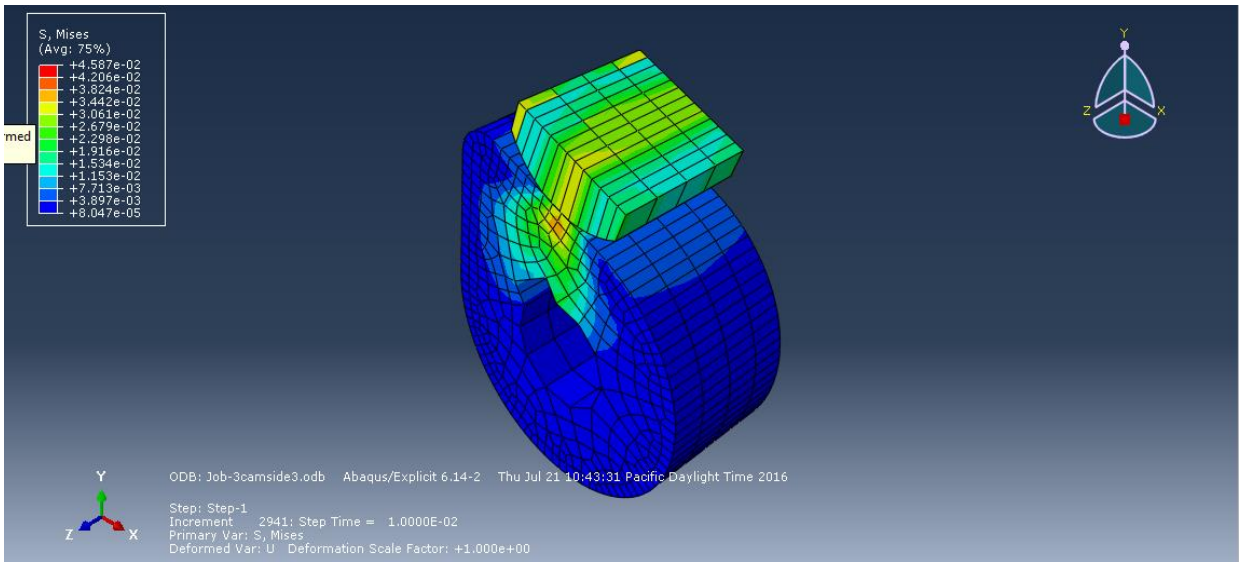

Fig 4.9 Distribution of von misses stress at the cam flank

Numerical value of the contact pressure resulted from abaqus is maximum: +5.588e-01MPa.

Cam lobe

The figure bellow shows the contour plot of distribution of von misses stress along the cam flank surface when the roller is in contact with the cam lobe surface.

Numerical value of the von misses stress resulted from abaqus is maximum: +5.130e-02 MPa which is well below the Yield strength of the material.

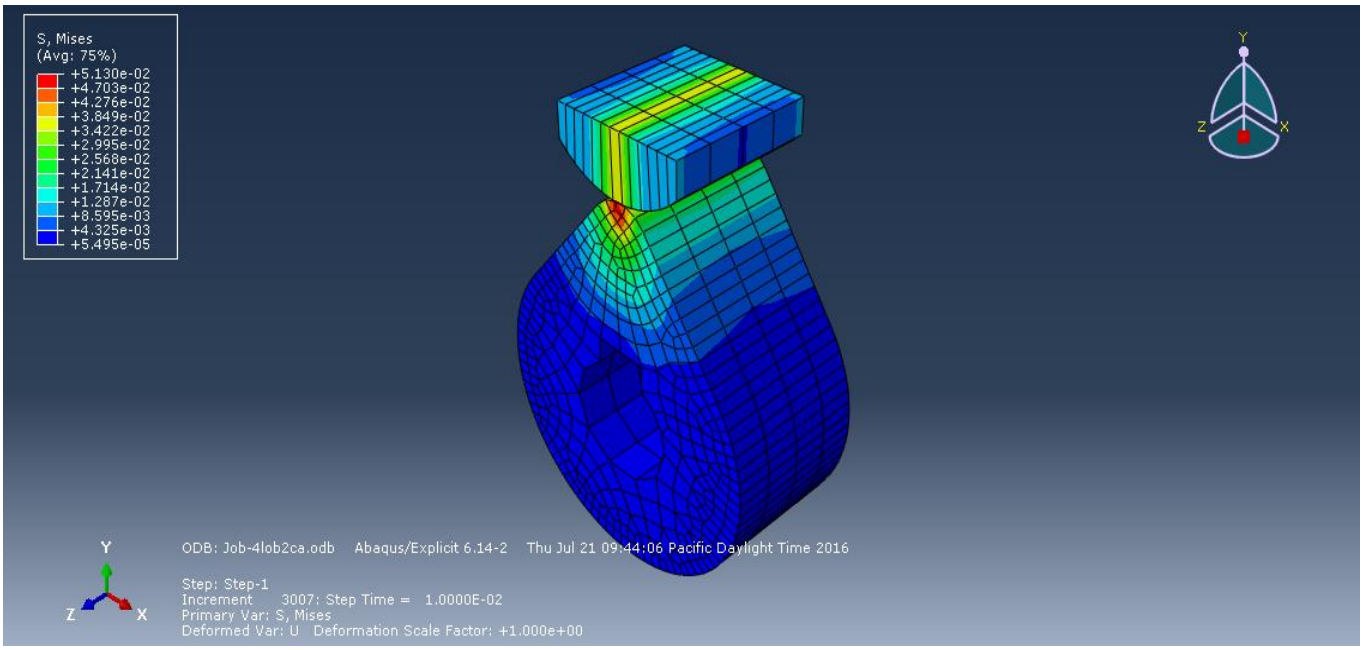

Fig 4.10 Distribution of von misses stress at the cam lobe

Numerical value of the contact pressure resulted from abaqus is maximum: +2.421e-01MPa.

- ABAQUS simulation at weight present of 2% Nano TiO_2-Al Cam

Cam Basic Circle

The figure bellow shows the contour plot of distribution of von misses stress along the cam basic circle surfaces when the roller is in contact with the cam basic circle surface.

Numerical value of the von misses stress resulted from abaqus is maximum: +4.634e-02MPa. Which is safe for the material.

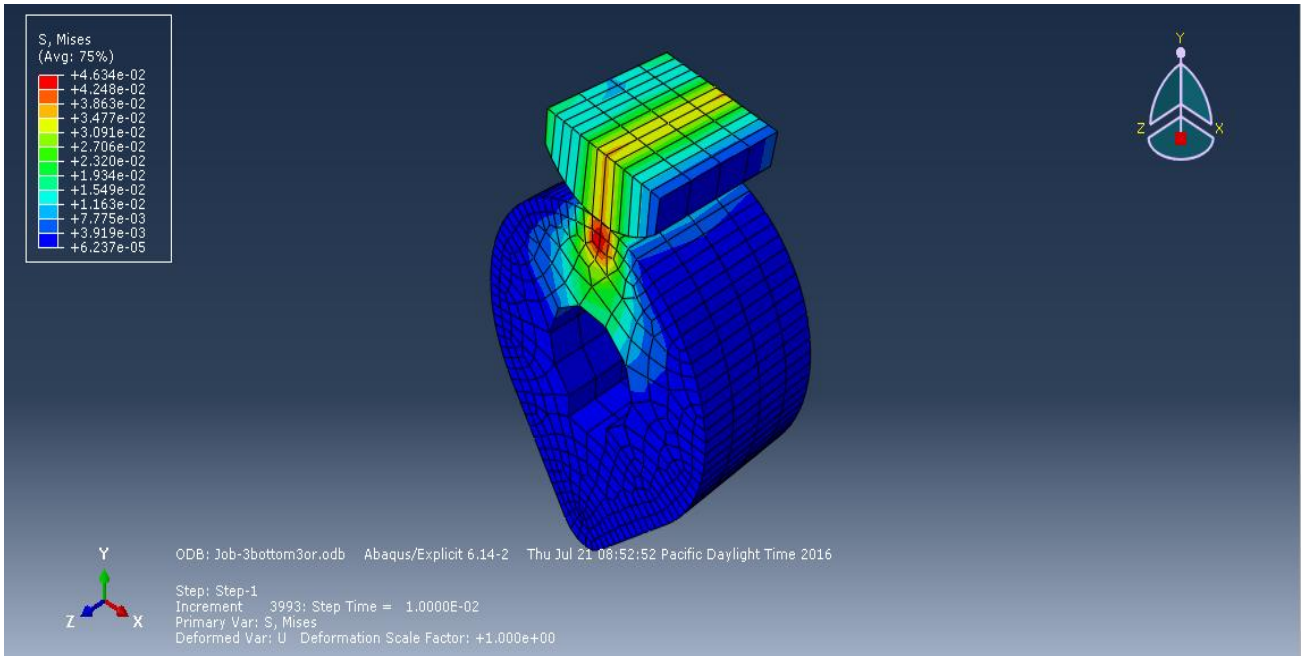

Fig 4.11 Distribution of von misses stress at the cam basic circle

Numerical value of the contact pressure resulted from abaqus is maximum: +9.523e-02MPa.

Cam Flank

The figure bellow shows the contour plot of distribution of von misses stress along the cam flank surface when the roller is in contact with the cam flank surface.

Numerical value of the von misses stress resulted from abaqus is maximum: +4.723e-02MPa which is safe for the material.

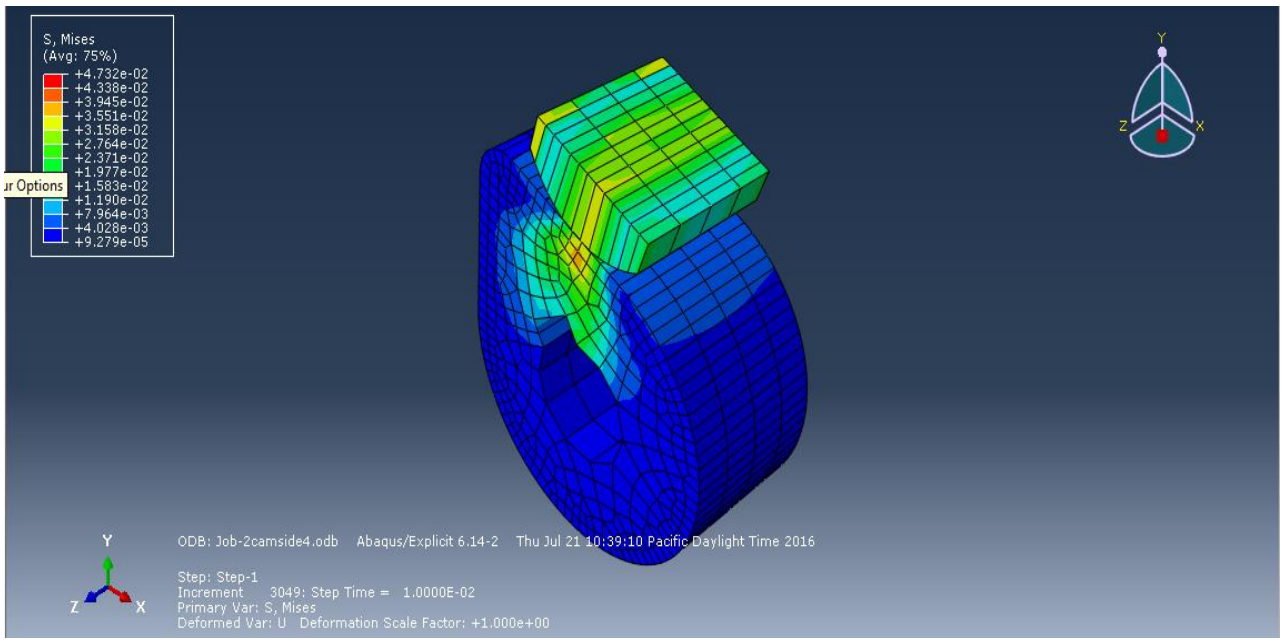

Fig 4.12 Distribution of von misses stress at the cam flank

Numerical value of the contact pressure resulted from abaqus is maximum: +5.714e-01MPa.

Cam lobe

The figure bellow shows the contour plot of distribution of von misses stress along the cam flank surface when the roller is in contact with the cam lobe surface.

Numerical value of the von misses stress resulted from abaqus is maximum: +5.206e-02 MPa which is also safe.

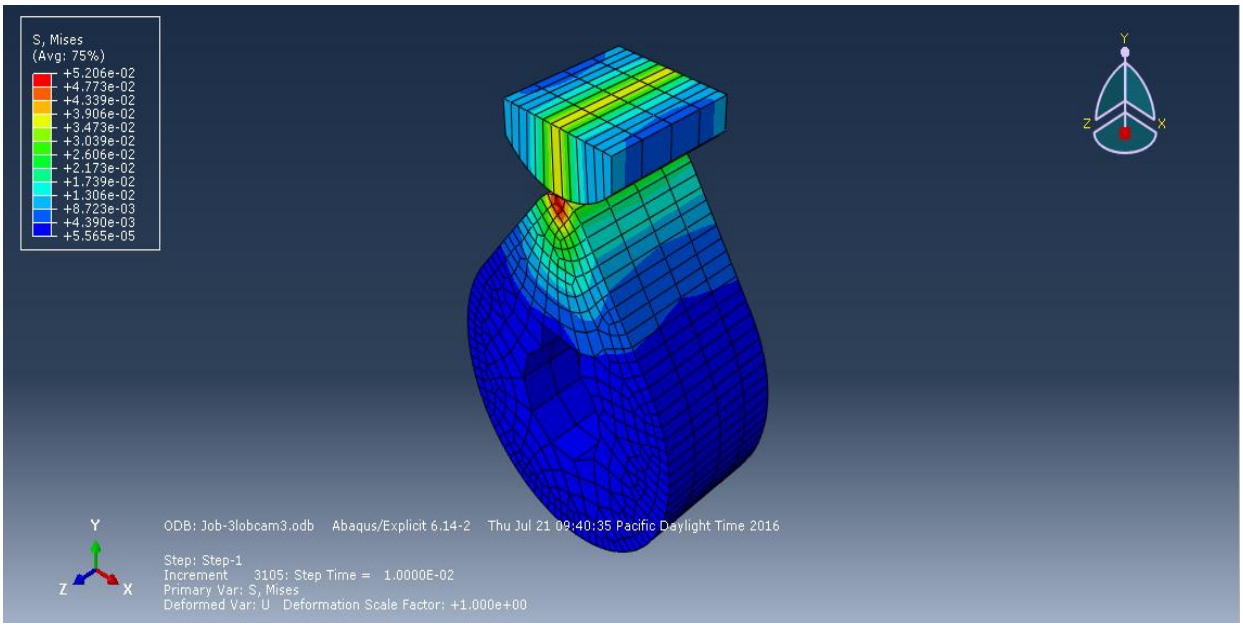

Fig 4.13 Distribution of von misses stress at the cam lobe

Numerical value of the contact pressure resulted from abaqus is maximum: +2.432e-01MPa.

- ABAQUS simulation at weight present of 1% Nano TiO_2-Al Cam

Cam Basic Circle

The figure bellow shows the contour plot of distribution of von misses stress along the cam basic circle surfaces when the roller is in contact with the cam basic circle surface.

Numerical value of the von misses stress resulted from abaqus is maximum: +4.540e-02MPa again within the safe loading condition of the material.

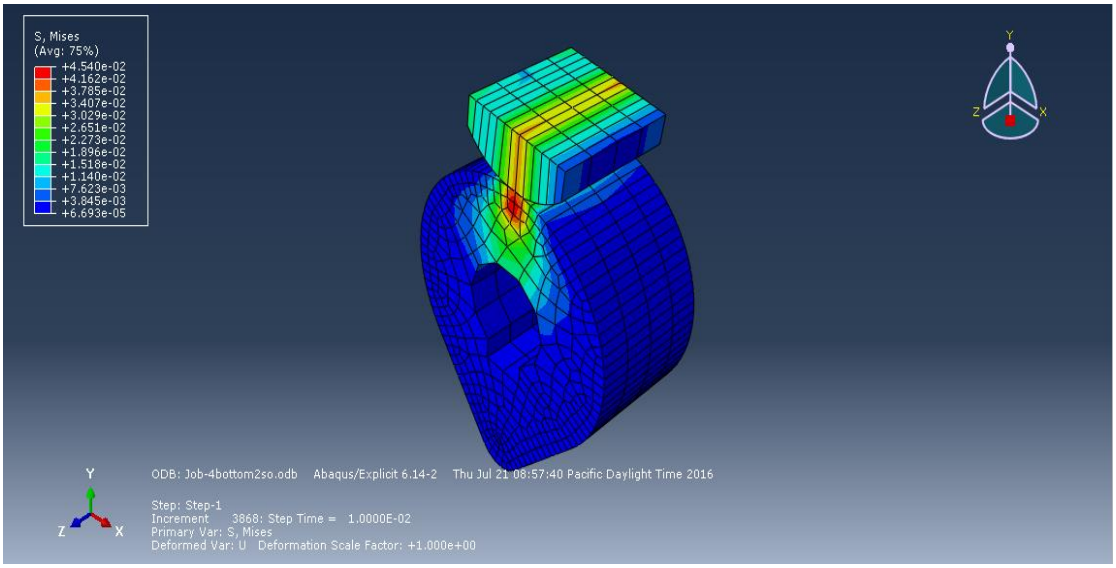

Fig 4.14 Distribution of von misses stress at the cam basic circle

Numerical value of the contact pressure resulted from abaqus is maximum: +9.565e-02MPa.

Cam Flank

The figure bellow shows the contour plot of distribution of von misses stress along the cam flank surface when the roller is in contact with the cam flank surface.

Numerical value of the von misses stress resulted from abaqus is maximum: +4.488e-02MPa again within the safe loading condition of the material.

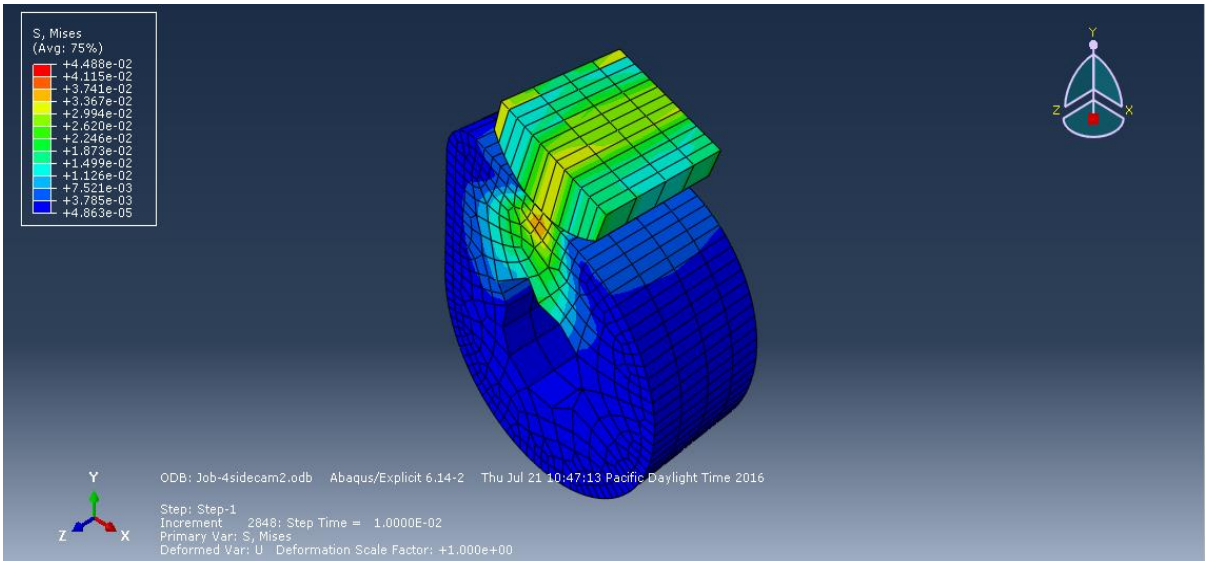

Fig 4.15 Distribution of von misses stress at the cam flank

Numerical value of the contact pressure resulted from abaqus is maximum: +5.727e-01MPa.

Cam lobe

The figure bellow shows the contour plot of distribution of von misses stress along the cam flank surface when the roller is in contact with the cam lobe surface.

Numerical value of the von misses stress resulted from abaqus is maximum: +5.336e-02 MPa again within the safe loading condition of the material.

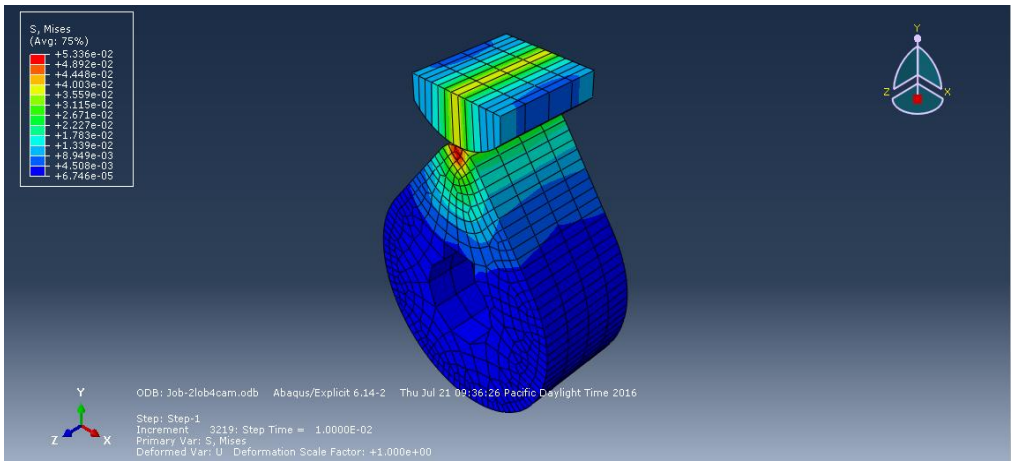

Fig 4.16 Distribution of von misses stress at the cam lobe

Numerical value of the contact pressure resulted from abaqus is maximum: +2.455e-01MPa.

- ABAQUS simulation at weight present of 10% Nano TiO_2-Al Cam

Cam Basic Circle

The figure bellow shows the contour plot of distribution of von misses stress along the cam basic circle surfaces when the roller is in contact with the cam basic circle surface.

Numerical value of the von misses stress resulted from Abaqus is maximum: +4.445e-02MPa which is safe loading condition.

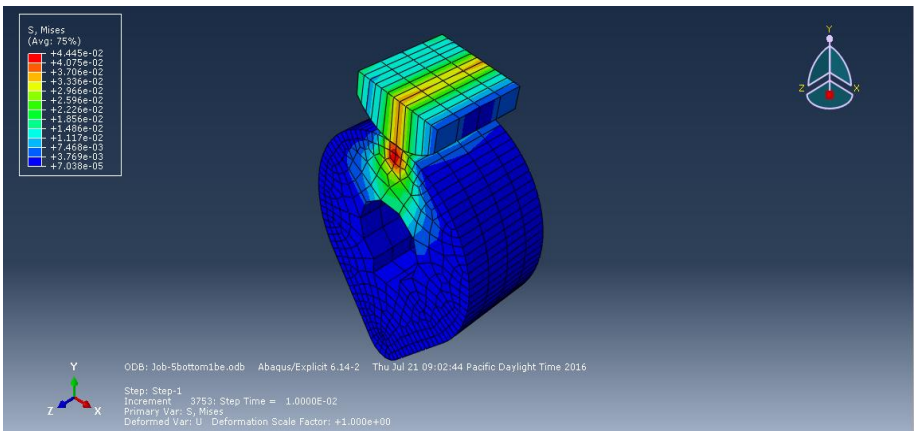

Fig 4.17 Distribution of von misses stress at the cam basic circle

Numerical value of the contact pressure resulted from abaqus is maximum: +10.124e-02MPa.

Cam Flank

The figure bellow shows the contour plot of distribution of von misses stress along the cam flank surface when the roller is in contact with the cam flank surface.

Numerical value of the von misses stress resulted from abaqus is maximum: +4.377e-02MPa which is safe loading condition.

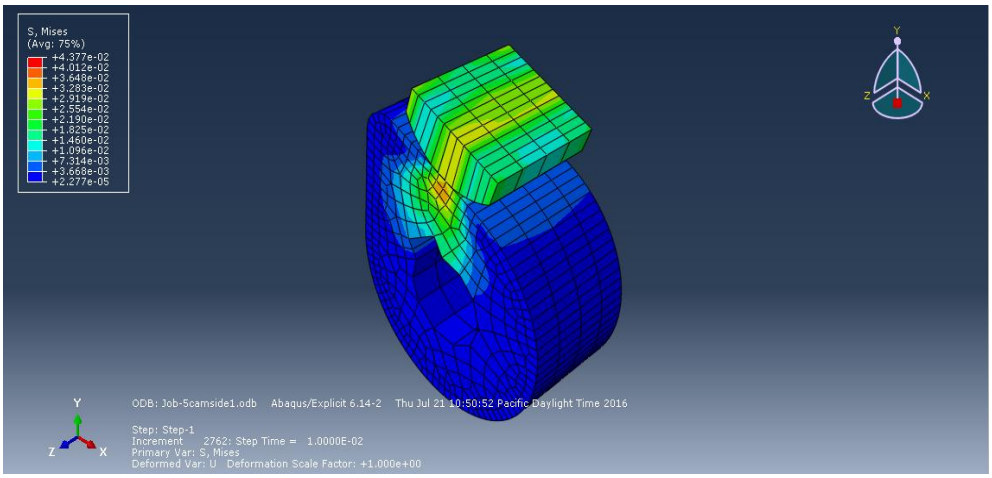

Fig 4.18 Distribution of von misses stress at the cam flank

Numerical value of the contact pressure resulted from abaqus is maximum: +7.241e-01MPa.

Cam lobe

The figure bellow shows the contour plot of distribution of von misses stress along the cam flank surface when the roller is in contact with the cam lobe surface.

Numerical value of the von misses stress resulted from abaqus is maximum: +5.453e-02 MPa which is safe loading condition.

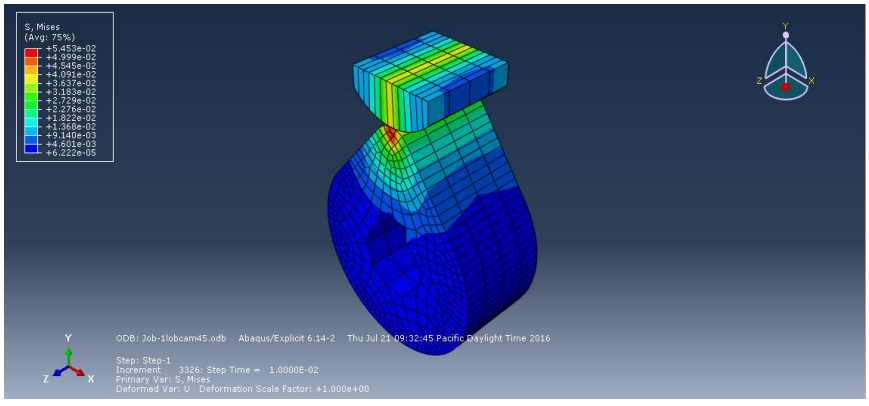

Fig 4.19 Distribution of von misses stress at the cam lobe

Numerical value of the contact pressure resulted from abaqus is maximum: +2.835e-01MPa.

- ABAQUS simulation at weight present of 4.5% Nano TiO_2-Al Cam

Cam Basic Circle

The figure bellow shows the contour plot of distribution of von misses stress along the cam basic circle surfaces when the roller is in contact with the cam basic circle surface.

Numerical value of the von misses stress resulted from abaqus is maximum: +5.927e+01MPa which is safe loading condition.

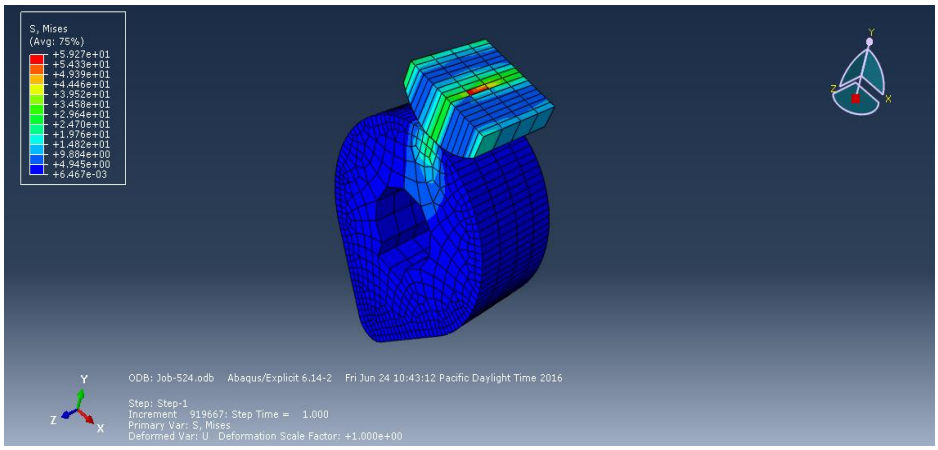

Fig 4.20 Distribution of von misses stress at the cam basic circle

Numerical value of the contact pressure resulted from abaqus is maximum: +9.015e-02MPa.

Cam Flank

The figure bellow shows the contour plot of distribution of von misses stress along the cam flank surface when the roller is in contact with the cam flank surface.

Numerical value of the von misses stress resulted from abaqus is maximum: +2.456e+01MPa.

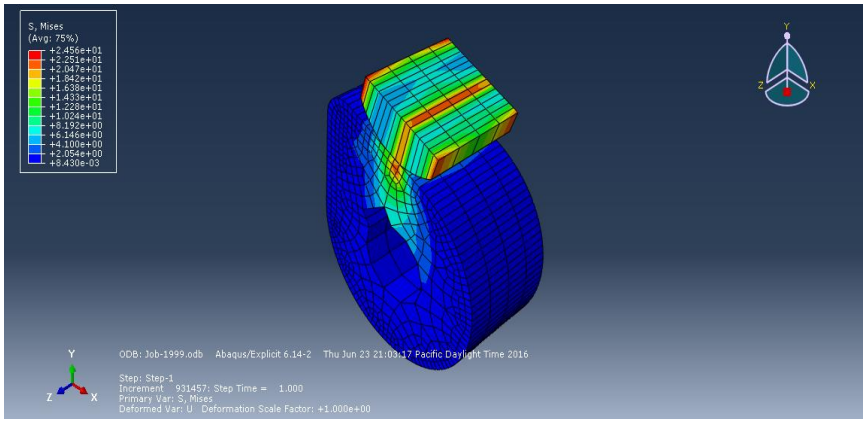

Fig 4.21 Distribution of von misses stress at the cam flank

Numerical value of the contact pressure resulted from abaqus is maximum: +4.325e-01MPa.

Cam lobe

The figure bellow shows the contour plot of distribution of von misses stress along the cam flank surface when the roller is in contact with the cam lobe surface.

Numerical value of the von misses stress resulted from abaqus is maximum: +1.049e+02 MPa which is safe loading condition.

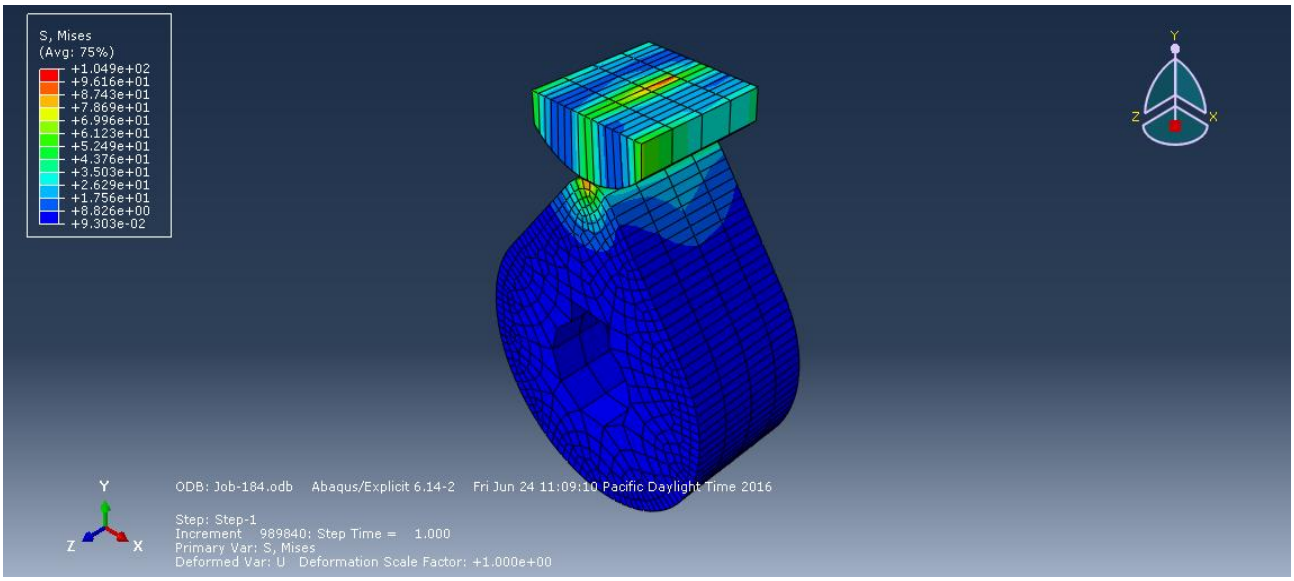

Fig 4.22 Distribution of von misses stress at the cam lobe

Numerical value of the contact pressure resulted from abaqus is maximum: +2.022e-01MPa.

4.1 Discussions

In this section, the weight loss of cam will be discussed and compared to the cam profile of Aluminum- SiC nano composite material at different weight percent.

- Weight loss of cam by wear in gram

The weight lost found by ABAQUS at the cam is calculated by using Archard's wear law. Result showed 0.006 gram of weight loss at test time duration of 2 hours and 4 wt % nano TiO_2. Compering this results with the new result obtained, it can be seen that for the same weight percentage of nano inclusion Nano Sic-Al cam shows better wear resistance capability than Nano-TiO_2. As we look the results below we can also observe that the optimum result for better wear resistant material using Nano-SiC, is obtained at 4.5 weight persente.

	Nano SiC-Al cam	Nano TiO_2-Al cam
10 % weight	0.0065 grams	0.008 grams
1 % weight	0.0095 grams	0.0075 grams
2 % weight	0.0078 grams	0.007 grams
3 % weight	0.0068 grams	0.0065 grams
4 % weight	**0.0075 grams**	**0.006 grams**
4.5 % weight		0.0055 grams

Table 4.1 Weights loose of cam at 2 kg and speed 300rpm

Figure bellow shows weight loose of cam at 2 kg and speed 300rpm.

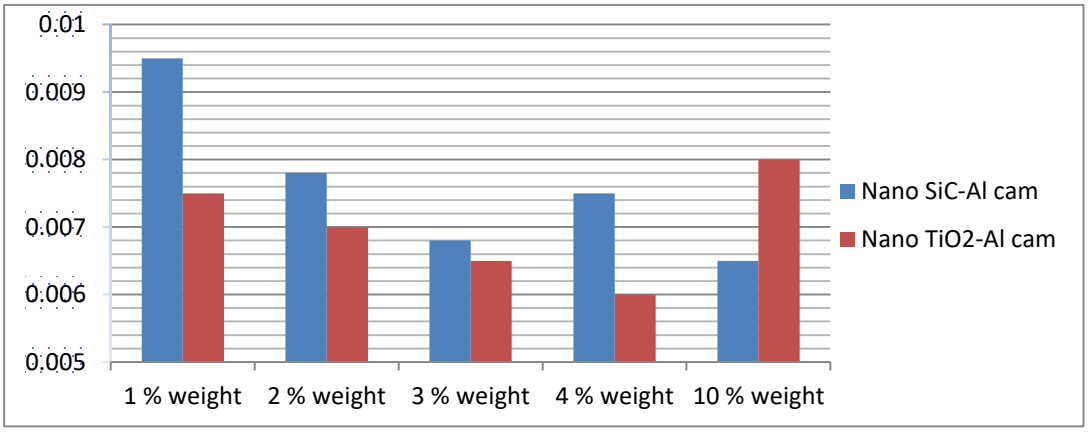

Fig 4.23 Weight loose of cam at 2 kg and speed 300rpm

From this result it can be concluded that TiO_2 has better wear rate at a range from 1 to 4.5 weight percent as shown,

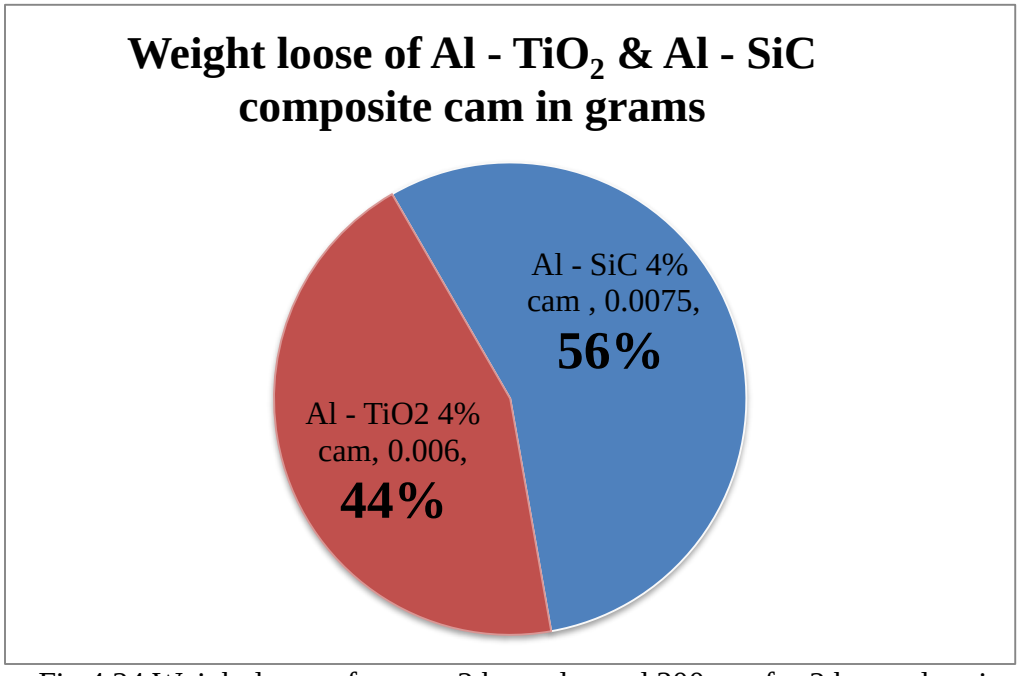

Fig 4.24 Weight loose of cam at 2 kg and speed 300rpm for 2 hours duration.

Chapter Five

Conclusion, Recommendation and Future work

5.1 Conclusion

A model has been developed for predicting cam and follower wear of composite cam for light duty vehicles.

Furthermore, comparison between of Aluminum 5083 4% Nano SiC with Aluminum 5083 4% Nano TiO_2 has been undertaken. The main conclusions which are obtained from these results are summarized below;

- Aluminum matrix Nano 4 wt. % TiO_2 composites have been successfully simulated by ABAQUS software 6.10CAE contact pressure shows higher result at the cam flank.
- Al- 4 wt. % nano TiO_2 composite shows highest value of surface hardness compared to Al – Nano SiC composite cam.
- At constant load of 2 kg and speed 300 rpm, cam with Al-4wt. % nano TiO_2 composites show lowest wear at the test duration of 6 hours by 0.0015grams less than Al-4 wt. % Nano SiC composites cam.
- The Al-TiO_2 composites can be used as alternative material for the cam other than Al-SiC composite cam due to better mechanical properties, lighter weight and better wear resistance.
- Wear rate of Al-TiO_2 composite cam can be improved further by few grams until weight percent of 4.5% TiO_2 composition. However, results show that, weight percent increase above 4.5% show greater wear loss.
- Since more addition of nano additives to a matrix material bring out less quality of the composite material, the result found from manufacturing nano silicon carbide with aluminum at weight percent of ten is unreliable.

5.2 Recommendation & Future Work

- Investigations should be conducted considering lubricants between the cam and follower contact and dispersion of the Nano fillers.
- The wear of cam and follower system should be conducted experimentally and the results should be compared with the ABAQUS results.
- Dispersion of the Nano fillers should also be considered.

References

[1] N. A.Thangarasua, "**Production and wear characterization of AA6082 -TiC surface**," 2014.

[2] H. Hua, "**Characterizing and Modeling Mechanical Properties of Nanocomposites revew and Evaluation**," p. 45, 2010.

[3] T. Tsutsui, "**Recent Technology of powder metallurgy and applications**," p. 9, 2015.

[4] R. a. Sagar, "**Fabrication of Metal Matrix Composite Automotive Parts**," p. 5, 1999.

[5] P. a. Vasin, "**Impact modeling for industrial cam follower system**," p. 23, 7 July 2013.

[6] R. R. P. k. s. Mayuresh singha, "**Development and Analysis of Al-Matrix Nano Composites fabricated by Powder metallurgy**," p. 7, 2015.

[7] Surappa, "**Wear analysis using FEM**," 2013.

[8] K. Shabani, "**study of the properties of Engine cam manufactured from cast iron**," 2012.

[9] a. B. O. a. R. D. SNAHNICAN Frantisek, "**Materials used in a construction of a camshaft mechanism**," p. 17, 2014.

[10] C. a. Werner, "**Nano composite materials and properties**," 1991.

[11] J. N. R. B. R. Mallikarjuna, "**Design Manufacturing and Cost Estimation of Camshaft Used In Two Wheeler**," p. 15, Feb 2014.

[12] J. T. a. N. B. a. R. H. M. W. G. G. D. Cooper, "**Design and manufacture of high performance hollow engine valves**," p. 12, 9 December 2014.

[13] E. E. N. Amal E. Nassar, "**Properties of aluminum matrix Nano composites**," p. 5, 22 April 2015.

[14] G. A. R. P. Dinesh Kumar Kolia, "**A Review on Properties, Behaviour and Processing Methods for Al-matrix composites**," p. 23, 2014.

[15] M. O. B. ,. A. Kenneth Kanayo Alaneme, "**Microstructure, mechanical and fracture properties**," p. 8, 22 January 2016.

[16] R. P. V. K. S. a. S. D. R. S. Ranaa, "**Development and Wear Analysis of Al- Nano SiC Composite**," 2015.

[17] H. F., "**use and benefits of nano composite materials**," 2013.

[18] S. a. Ramesh, "**study of nano particles on aluminium matrix**".

[19] S. a. Purohit, "**Effect of addition of nano particles on matrix materials**".

[20] Das, "**engine cam wear profile and manufacturing methods**," 2013.

[21] Purohit, "**Experimental study of engine cam wear**," 2014.

[22] R. a. Sannino, "**study of dry wear of cam shaft**," 1995.

[23] j. a. escobar, "**stress and fatigue analysis of svi-tested camshaft**," p. 110, november 2013.

[24] B. S. R.Ipeka, "**The dry wear profile of cam shaft**," p. 4, 23 September 2004.

[25] B. S. Ripeka, "**The dry wear profile of cam shaft**," p. 4, 23 September 2014.

[26] P. T. S. K. a. A. Nazaruddin, "**Effect of Addition of Nanoparticles**," p. 5, August 2015.

[27] L. O. A. A. Hurang Hua, "C**haracterizing and Modeling Mechanical Properties of Nanocomposites-Review and Evaluation**," p. 45, 2010.

[28] Parashkevova, "**Micropolar-based modeling of size effects on stiffness and yield stress**," p. 13, 23 Ovtober 2012.

[29] L. a. Per, "**Characterization of wear on a cam follower system in desil engine**," p. 13, March 2013.

[30] c. C. Juliano Savoy, "**contact pressure between cams and roller followers through FEM in assembled cam shafts**," p. 21, May 2013.

[31] J. M. K. K. J. Michalski, "**an experimental study of desile engine cam and follower with particular reference to properties of materials**," p. 17, 1999.

[32] M. H. B. Ghazalli, "**Finite Element analysis of cam and its follower contact stress mechanism.**," p. 13, 2007.

[33] Gibson, "**composite materials in automotives**," 2010.

[34] H. Clyne, "**Aluminium matrix nano composite manufacturing methodes**," 1996.

[35] Leif, "**Engine Cam manufacuring by using nano composites**," 2002.

[36] Totten, "**Dry wear of cam shaft in light weight vehicles**," 2006.

[37] Kala, "**Experimental study of Aluminium matriox nano titanium dioxide composite material**," 2014.

[38] R. R. Siddhartha Prabhakar, "**Analysis of tribological behavior of aluminium/B4C composite**," p. 10, 2014.

[39] L. L. A. S. Enrico Radia, "**Analytical modelling of the pullout behavior of synthetic fibres,**" p. 8, 2015.

[40] D. K. M. a. C. S. Ganesh Khandoori1, "**Sliding behaviour of aluminium metal matrix composite reinforced with nano titanium dioxide**," p. 7, 2015.

[41] D. K. Xiaozhen Qu, "**Kinematic design and analysis of a four-bar linkage-type continuously**," p. 15, 17 August 2012.

[42] J. T. B. D. Cooper, "**Design and manufacture of high performance hollow engine valves by additive layer Manufacturing**," p. 12, December 2014.

[43] S. B. M. C. C. Per Lindholm, "**Characterisation of wear on a cam follower system in a diesel engine**," p. 9, 2003.

[44] C. Park, "**Cam follower friction**," 2010.

[45] P. clyde h . moon, "**cam design**," USA, commercial cam division,emersion electric company, 2013, p. 69.

[46] D. et, "**Aluminium matrix nano composites**," 2010.

[47] Gibson, "**composite materials for automotives**".

[48] J. M. K. K. J. Michalski, "**An experimental study of diesel engine cam and follower wear**," p. 12, 17 February 2000.

[49] W. Z. X. Z. Y. C. Jie Guo, "**Dynamic and exciting analysis with modal characteristics for nano composites**," p. 19, 25 March 2014.

[50] J. M. K. K. J. Michalski, "**An experimental study of diesel engine cam and follower**," p. 12, february 2013.

[51] L. C. et, "**Nano composite materials**".

[52] P. L. b. Nagaraj Nayaka, "**Predictions of cam follower wear in diesel engines**," p. 12, 10 May 2005.

[53] S. S. D. K. Pardeep Sharmaa, "**alloycomposites production and some properties of**

Si3N4 reinforced aluminium," p. 8, 1 August 2015.

[54] G. S. R. E. S. Arumugam, "**An experimental study of Bio-lubricant-biodiesel combination of rapeseed oil**," p. 10, 23 may 2014.

[55] S. V. a. T. Wallner, "**Hydrogen-fueled internal combustion engines**," p. 38, 18 august 2009.

[56] I. A. R. N. K. R. Sefiu Adekunle Bello, "**fractography and Study of tensile properties**," p. 9, 6 october 2015.

[57] M. b. M. S. S. Mohammadi-Aghdam, "**Kinetic modeling of BB41 photocatalytic treatment**," p. 10, 17 October 2013.

[58] Tahamtan, "**Enhanced tensile properties of aluminium matrix**," p. 25, 2015.

[59] M. M. a. N. U. Abdullahia, "**Wear mechanisms map of CNT-Al nano-composite**," p. 7, 2013.

[60] B. B. L. R. Vicente Macián, "**Assessment of the effect of low viscosity oils usage on a light duty**," 16 June 2014.

Appendix: 1

Car Model	Honda - SOHC
Engine Type	In its late V6 Engine, 3.5 liter
Number of valve per cylinder	4
Torque	271hp/254lb-ft

Table: Car model for single overhead cam (SOHC)

Appendix: 2

MatLab Modeling

alu_final.m

```
function [Kf,Gf]= alu_final
Gj=28.3e9;
vj=0.4;
Ej=Gj*2*(1+vj);
Kj=Ej/(3*(1-(2*vj)));
vo=0.35;
Go=26.6e9;
Eo=72e9;
lam=(Eo*vo)/((1+vo)*(1-(2*vo)));
Ko=lam+((2/3)*Go);
a=10e-9;
l=2*a;
bg=(1+((20e-9^2)/(2*a*l)));
syms rj rk;
for rj= (20e-9);
    q=10;
k=(1:10);
 rk=rj+(a.*(1-((k-1)./q)));

Kk=Ko+(Kj-Ko).*((rj+a-rk)/a).^bg;
Gk=Go+(Gj-Go).*((rj+a-rk)./a).^bg;
Ck=(rj+(a.*((q-k+1)./q).^3))-(rj+(a.*((q-k)./q).^3))./((rj+a).^3);
Ck1=(rj./(rj+a));
syms W1 W2 Ke Ge;
W1=sum(Ck./(1-(((3*Ke)./((3*Ke)+(4*Ge))).*(1-(Kk./Ke)))));
W2=sum(Ck./(1-(((2*((3*Ke)+(6*Ge)))./(5*((3*Ke)+(4*Ge)))).*(1-(Gk./Ge))))));
[Ke,Ge]=solve(W1-1==0,W2-1==0,Ke,Ge);

Csum=0.07;
Co=1-Csum;
```

```
Ci=0.6;
Ke=6.1970e10;
Ge=0.6490e10;
ao=((3*Ko)/((3*Ko)+(4*Go)));
bo=((6*(Ko+(2*Go)))./(5*((3*Ko)+(4*Go))));
Kc=((Ko*(1+(((Csum)*(Ke-Ko))/(Co*ao*(Ke-Ko)+Ko)))));
Gc=((Go.*(1+(((Csum).*(Ge-Go))./(Co.*bo.*(Ge-Go)+Go)))));


syms Kf Gf F F1
F=sum(Ci./(1-((3*Kf)./((3*Kf)+(4*Gf)).*(1-(Kc/Kf)))));
F1=sum(Ci./(1-((2*((3*Kf)+(6*Gf)))./(5*(3*Kf)+(4*Gf))).*(1-(Gc./Gf))));
[Kf,Gf]=solve(F==1,F1==1,Kf,Gf)
end
```